

RESEARCH ARTICLE

The ESCRT-III machinery participates in the production of extracellular vesicles and protein export during *Plasmodium falciparum* infection

Yunuen Avalos-Padilla^{1,2,3*}, Vasil N. Georgiev³, Elena Lantero^{1,2}, Silvia Pujals^{1,4}, René Verhoef⁵, Livia N. Borgheti-Cardoso¹, Lorenzo Albertazzi^{1,6}, Rumiana Dimova³, Xavier Fernàndez-Busquets^{1,2*}

1 Institute for Bioengineering of Catalonia (IBEC), The Barcelona Institute of Science and Technology (BIST), Barcelona, Spain, **2** Barcelona Institute for Global Health (ISGlobal, Hospital Clínic-Universitat de Barcelona), Barcelona, Spain, **3** Department of Theory and Bio-Systems, Max Planck Institute of Colloids and Interfaces, Science Park Golm, Potsdam, Germany, **4** Department of Electronics and Biomedical Engineering, Faculty of Physics, Universitat de Barcelona, Barcelona, Spain, **5** Computational Biology Group, Eindhoven University of Technology, Eindhoven, The Netherlands, **6** Department of Biomedical Engineering and the Institute for Complex Molecular Systems, Eindhoven University of Technology, Eindhoven, The Netherlands

* yavalos@ibecbarcelona.eu (YA-P); xfernandez_busquets@ub.edu (XF-B)



OPEN ACCESS

Citation: Avalos-Padilla Y, Georgiev VN, Lantero E, Pujals S, Verhoef R, N. Borgheti-Cardoso L, et al. (2021) The ESCRT-III machinery participates in the production of extracellular vesicles and protein export during *Plasmodium falciparum* infection. *PLoS Pathog* 17(4): e1009455. <https://doi.org/10.1371/journal.ppat.1009455>

Editor: Isabelle Coppens, Johns Hopkins University Bloomberg School of Public Health, UNITED STATES

Received: September 24, 2020

Accepted: March 8, 2021

Published: April 2, 2021

Copyright: © 2021 Avalos-Padilla et al. This is an open access article distributed under the terms of the [Creative Commons Attribution License](https://creativecommons.org/licenses/by/4.0/), which permits unrestricted use, distribution, and reproduction in any medium, provided the original author and source are credited.

Data Availability Statement: All relevant data are within the manuscript and its [Supporting Information](#) files.

Funding: YA.-P. and L.N.B.-C. received financial support provided by the European Commission under Horizon 2020's Marie Skłodowska-Curie Actions COFUND scheme (712754) and by the Severo Ochoa programme of the Spanish Ministry of Science and Competitiveness [SEV-2014-0425]

Abstract

Infection with *Plasmodium falciparum* enhances extracellular vesicle (EV) production in parasitized red blood cells (pRBCs), an important mechanism for parasite-to-parasite communication during the asexual intraerythrocytic life cycle. The endosomal sorting complex required for transport (ESCRT), and in particular the ESCRT-III sub-complex, participates in the formation of EVs in higher eukaryotes. However, RBCs have lost the majority of their organelles through the maturation process, including an important reduction in their vesicular network. Therefore, the mechanism of EV production in *P. falciparum*-infected RBCs remains to be elucidated. Here we demonstrate that *P. falciparum* possesses a functional ESCRT-III machinery activated by an alternative recruitment pathway involving the action of PfBro1 and PfVps32/PfVps60 proteins. Additionally, multivesicular body formation and membrane shedding, both reported mechanisms of EV production, were reconstituted in the membrane model of giant unilamellar vesicles using the purified recombinant proteins. Moreover, the presence of PfVps32, PfVps60 and PfBro1 in EVs purified from a pRBC culture was confirmed by super-resolution microscopy and dot blot assays. Finally, disruption of the *PfVps60* gene led to a reduction in the number of the produced EVs in the KO strain and affected the distribution of other ESCRT-III components. Overall, our results increase the knowledge on the underlying molecular mechanisms during malaria pathogenesis and demonstrate that ESCRT-III *P. falciparum* proteins participate in EV production.

(2015–2019)]. S.P. and L.A. acknowledge the financial support by the Spanish Ministry of Science and Innovation (PID2019-109450RB-I00/AEI/10.13039/501100011033), European Research Council/Horizon 2020 (ERC-StG-757397), "la Caixa" Foundation (ID 100010434), and by the Generalitat de Catalunya (through the CERCA program and 2017 SGR 01536). This research was funded by the Ministerio de Ciencia, Innovación y Universidades, Spain (which included FEDER funds), grant numbers BIO2014-52872-R and RTI2018-094579-B-I00. This work is part of the MaxSynBio consortium, which was jointly funded by the Federal Ministry of Education and Research of Germany and the Max Planck Society. ISGlobal and IBEC are members of the CERCA Programme, Generalitat de Catalunya. This research is part of ISGlobal's Program on the Molecular Mechanisms of Malaria which is partially supported by the Fundación Ramón Areces. We acknowledge support from the Spanish Ministry of Science, Innovation and Universities through the "Centro de Excelencia Severo Ochoa 2019-2023" Program (CEX2018-000806-S). The funders had no role in study design, data collection and analysis, decision to publish or preparation of the manuscript.

Competing interests: The authors have declared that no competing interests exist.

Author summary

Malaria is a disease caused by *Plasmodium* parasites that is still a leading cause of death in many low-income countries, and for which currently available therapeutic strategies are not succeeding in its control, let alone eradication. An interesting feature observed after *Plasmodium* invasion is the increase of extracellular vesicles (EVs) generated by parasitized red blood cells (pRBCs), which lack a vesicular trafficking that would explain EV production. Here, by combining different approaches, we demonstrated the participation of the endosomal sorting complex required for transport (ESCRT) machinery from *Plasmodium falciparum* in the production of EVs in pRBCs. Moreover, we were able to detect ESCRT-III proteins adjacent to the membrane of the host and in EVs purified from a pRBC culture, which shows the export of these proteins and their participation in EV production. Finally, the disruption of an ESCRT-III associated gene, *Pfyps60*, led to a significant reduction in the amount of EVs. Altogether, these results confirm ESCRT-III participation in EV production and provide novel information on the *P. falciparum* protein export mechanisms, which can be used for the development of new therapeutic strategies against malaria, based on the disruption of EV formation and trafficking.

Introduction

Plasmodium spp is the parasite responsible for malaria, a disease that, despite the efforts done to control it, still represents a health problem worldwide particularly in low-income countries [1]. During *Plasmodium* infection, an elevated number of extracellular vesicles (EVs) from numerous cellular sources are circulating in the plasma [2], the amount of which correlates with the severity of the disease [2–5]. Despite of its high impact in the development of the pathology, the precise mechanism of EV formation in the infected red blood cells (RBCs) remains to be elucidated. One of the yet unsolved enigmas of malaria pathophysiology is how mature RBCs are able to release high amounts of EVs after *Plasmodium* infection, since they are biochemically simple compared to other eukaryotic cells and lack a normal vesicular network. It has been suggested that *Plasmodium* uses its own protein network to establish a vesicular trafficking for the export of an arsenal of virulence factors which contributes to the establishment of the parasite in the host cells [6].

In higher eukaryotes, EVs are generated and transported to their final destination by the endomembrane system [7]. Trafficking within the endomembrane system is crucial for the functional communication between different compartments in eukaryotic cells [8]. Depending on their origin and size, EVs can be classified into two major classes: exosomes and microvesicles. Exosomes refer to endosome-derived vesicles with a diameter typically of 30–50 nm that are generated following the fusion of multivesicular bodies (MVBs) with the plasma membrane. On the other hand, microvesicles are plasma membrane-derived vesicles which result from direct membrane shedding and exhibit a size from 100 nm up to 1 μ m [9].

MVBs are shaped after the formation of intraluminal vesicles (ILVs) in early endosomes [10]. The genesis of ILVs relies on the sequential action of the endosomal sorting complex required for transport (ESCRT), which consists of four protein complexes termed ESCRT-0, ESCRT-I, ESCRT-II, ESCRT-III and a set of accessory proteins [11,12]. The best-described mechanism of ESCRT action begins with the recognition of mono-ubiquitinated proteins by ESCRT-0 [13], which then activates the recruitment of ESCRT-I [14] and ESCRT-II [15] that are responsible for membrane deformation into buds [16,17]. Finally, the polymerization of ESCRT-III begins with the binding of Vps20 to the invaginated membrane, which recruits the

rest of the ESCRT-III members to the bud neck and the nascent vesicle is closed [16,18,19]. The membrane fission, protein dissociation and recycling of the machinery depends on the participation of the Vps4 AAA-ATPase [20]. Among all the sub-complexes, ESCRT-III (composed by Vps20, Snf7/Vps32, Vps24 and Vps2) and its accessory proteins (Vps4, Vta1, Vps60, Alix) are also involved in other important membrane-scission mechanisms, including virus budding, cytokinesis, nuclear envelope remodeling and exosome biogenesis among others (see review in [21]). All of these processes share the same topology where the nascent vesicle buds away from the cytosol, contrary to the topology observed in clathrin-coated vesicles [22].

The ESCRT machinery is highly conserved across the eukaryotic lineage; however, strictly intracellular protists, like *Plasmodium spp.*, are devoid of ESCRT-0, -I and -II sub complexes [23]. In the case of *Plasmodium* and other organisms that lack the full ESCRT machinery, it is plausible that other proteins trigger ESCRT-III activation. In this regard, Alix, a Bro1-domain protein, binds directly to Vps32 and triggers the formation of ESCRT-III polymers, leading to ILVs formation in humans [24]. Whether a similar mechanism, alternative to the canonical ESCRT-III pathway, exists in *Plasmodium* remains to be determined.

Previous *in silico* assays showed that *Plasmodium falciparum*, the deadliest human malaria parasite species, possesses at least two putative proteins from the ESCRT-III complex: Vps2 and Vps32/Snf7 [23,25]. Additionally, the ATPase Vps4, an accessory protein of the ESCRT-III complex, was found in the cytoplasm of *P. falciparum* during the trophozoite blood stage [26]. Moreover, PFVps4 retained its function in MVB formation when transfected into *Toxoplasma gondii* and COS cells, thus strongly suggesting the existence of a functional ESCRT machinery in *P. falciparum* that mediates the production of MVBs [26].

Since *P. falciparum* lacks upstream ESCRT complexes, here we have investigated the presence of a putative Bro1-domain protein involved in an alternative ESCRT-III recruitment pathway. In addition, we have studied the participation of a minimal ESCRT-III machinery in EV biogenesis during *Plasmodium* infection. Overall, our findings provide an important insight into export mechanisms in *Plasmodium*-infected RBCs mediated by the parasite.

Results

Plasmodium falciparum possesses a Bro1 domain-containing protein

A previous *in silico* study in the *P. falciparum* genome revealed the presence of only six out of the 26 ESCRT-machinery proteins present in humans. The study showed that the genome of *P. falciparum* encodes four Snf7-domain containing proteins [23], a conserved feature in all ESCRT-III members [27]. Based on our *in silico* Basic Local Alignment Search Tool (BLAST) analysis, the four proteins were denoted as PfVps32, PfVps60, PfVps2 and PfVps46 (S1 Table).

The absence of ESCRT-I- and -II-associated genes and of a Vps20 homologue in the genome of *P. falciparum*, suggested the existence of an alternative recruitment pathway in the parasite. Hence, we explored the presence of a Bro1 domain-containing protein in *P. falciparum* that could bind directly to the Snf7 candidates and trigger the activation of the ESCRT-III system in this parasite, similarly to the process regulated by Alix in humans [24]. An *in silico* search of the *P. falciparum* genome (<http://www.plasmodb.org>) showed that the parasite has a unique Bro1-containing homologue termed PF3D7_1224200 (hereafter referred to as PfBro1) with a 3175 bp open reading frame and carrying 4 introns. The open reading frame of PfBro1 encodes an 819 amino acid protein with a predicted molecular mass of 98,714 Da. Our further assays revealed that the amino acid sequence of full-length PfBro1 had an identity of 21.8% with Alix, whereas the Bro1 domain in PfBro1 exhibited a 23.6% identity with its human homologue. Despite of this low amino acid conservation, we identified several conserved residues of the two charged polar clusters which, in several Bro1 homologues, stabilize the Bro1

domain [28]. These residues include R51, Y70 and E116 from the first cluster, and E187 and K246 from the second cluster (S1 Fig). Importantly, PfBro1 showed conservation of the residue I144 (S1 Fig), which has been demonstrated to directly participate in the binding of Vps32 in *Saccharomyces cerevisiae* [28]. We then performed additional tertiary structure prediction assays, revealing that the full-length PfBro1 has a hypothetical hydrophobic tail in its C-terminal region (S2 Fig), which makes it a good candidate for the recruitment of ESCRT-III components at the level of the membrane. Moreover, a pentameric *Plasmodium* export element (PEXEL) motif was found in the N-terminal sequence of PfBro1 (S1 Fig, double underline), which is present in many exported proteins in *P. falciparum* [29].

PfBro1 and PfVps32 are exported to the cytoplasm of the erythrocyte

In order to continue our characterization of the ESCRT-III machinery in *P. falciparum*, we focused on resolving the putative role of three proteins: (1) PfVps32, the most abundant protein in the ESCRT machinery. (2) PfVps60, whose human homologue, CHMP5, is able to bind directly to Brox [30] (a Bro1-containing protein found in exosomes of human urine [31]), and redistribute it to membrane-enriched fractions [30]; and (3) PfBro1 as their potential recruiter and activator. Consequently, genes encoding the aforementioned proteins were chemically synthesized and cloned into the appropriate vector, to induce and purify the corresponding proteins. Coomassie blue-stained gels confirmed the integrity of the purified proteins (S3 Fig) which were used for the rest of the experiments.

Rabbit polyclonal antibodies against the purified recombinant proteins were generated and used to detect their presence in extracts obtained from *P. falciparum* cultures during the intraerythrocytic stage. In Western blot assays, the specific antibodies recognized PfVps32, PfVps60 and PfBro1 recombinant proteins from induced bacterial lysates, and *Plasmodium* native proteins in pRBC lysates 30 hours post invasion (hpi) (S3 Fig). Using parasite extracts, antibodies against PfVps32 and PfBro1 detected bands of the expected molecular weights (26 and 98 kDa, respectively). However, similarly to other Snf7-containing proteins [32,33], PfVps60 was detected with a higher molecular weight (46 kDa) than that predicted by the amino acid sequence (27 kDa) (S3 Fig). Nevertheless, bacterially expressed PfVps60 also migrated in an identical manner, suggesting that the highly charged nature of the proteins could influence their electrophoretic migration [32]. Preimmune serum used as a control did not reveal any band in *P. falciparum* extracts (S3 Fig).

To determine the localization of the studied proteins, parasites synchronized at early (8 hpi) or late stages (40 hpi) were lysed using a detergent fractionation approach. This technique allowed us to obtain three different fractions: (1) saponin fraction, containing RBC cytosolic proteins, (2) Triton X-100 fraction, enriched in proteins from membranes and *P. falciparum* organelles, and (3) radio-immunoprecipitation assay (RIPA) buffer fraction, where most cytoskeletal components are present (Fig 1A). To assess the purity of the isolated fractions, we used antibodies against glycophorin A (GPA), which is the major intrinsic membrane protein of the erythrocyte. As expected, GPA was absent from the saponin fraction but was detected in the Triton X-100 and RIPA fractions of both RBCs and pRBCs. On the other hand, antibodies against spectrin revealed the presence of this cytoskeletal protein only in the RIPA fraction of infected and non-infected RBCs.

PfVps32 and PfBro1 were present in the saponin extracts of both early and late stages after invasion, indicating their export to the RBC cytoplasm. In the RIPA buffer fraction, PfBro1 was found in early and late stages, while PfVps32 and PfVps60 were mainly present in late stages. Finally, all three proteins were found in the Triton X-100 extracts of both stages. As control, we used the *P. falciparum* heat shock protein 70 (PfHSP70), which was detected in all

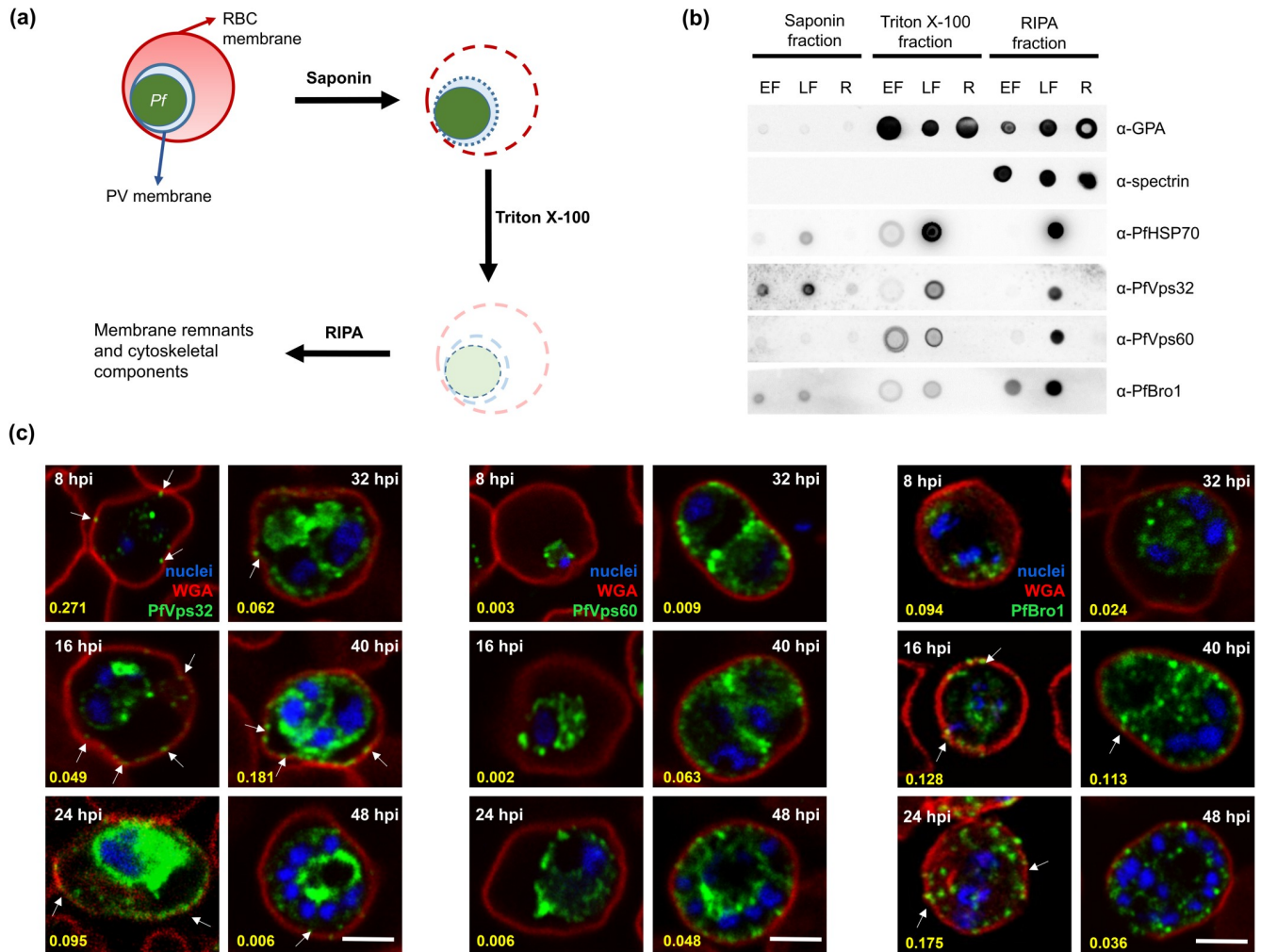


Fig 1. Expression and localization of PfVps32, PfVps60 and PfBro1 during the *P. falciparum* intraerythrocytic cycle. (a) Diagram illustrating the approach for the differential detergent fractionation protocol used for obtaining saponin, Triton X-100 and RIPA fractions. (b) Dot-blot assays performed with the different pRBCs extracts at early (8 hpi, EF) and late forms (40 hpi, LF) after RBC invasion using the different antibodies as indicated. As control, extracts obtained from non-infected RBCs (R) were also included. (c) Human erythrocytes were infected with *P. falciparum* and fixed at different hpi. PfVps32, PfVps60 or PfBro1 (green) were detected by indirect confocal immunofluorescence microscopy and WGA (red) was used to label the RBC plasma membrane. Cell nuclei were visualized with Hoechst 33342 (blue). Arrows show protein-labeled puncta adjacent to the membrane of the pRBCs. Numbers in yellow indicate Manders' overlap coefficients used to evaluate co-localization between WGA and each protein tested. Scale bar: 5 μ m.

<https://doi.org/10.1371/journal.ppat.1009455.g001>

fractions of pRBCs except in the RIPA fraction at early stages. Neither ESCRT-III proteins nor the PfHSP70 control were present in protein fractions obtained from non-parasitized RBCs (Fig 1B). Western blot results indicated that PfVps32, PfVps60 and PfBro1 are expressed throughout the intraerythrocytic cycle (S4 Fig). Interestingly, antibodies against PfBro1 and PfVps60 detected more than one band in some fractions, which probably indicates a proteolytic processing of the proteins or their association to ligands possibly related with their function or degradation (S4 Fig). However, more experiments are necessary to prove this.

Immunofluorescence assays showed that PfVps32, PfVps60 and PfBro1 were localized in the cytoplasm of the parasite, inside the parasitophorous vacuole (PV) (Fig 1C). In the case of PfVps32 and PfBro1, puncta stained with their respective antibodies were observed in the cytoplasm of parasitized erythrocytes outside the PV (Fig 1C, arrows), some of them close to the RBC membrane. To examine whether these structures are exported to the parasitized RBC

(pRBC) plasma membrane, lectins present in the RBC surface were labeled with wheat germ agglutinin (WGA) and Manders' overlap coefficients were used to assess co-localization (Fig 1C, yellow numbers). There was no significant co-localization between WGA and the proteins, indicating that PfVps32- and PfBro1-labeled puncta localized adjacent to the surface lectin. The polyclonal antibodies raised against PfVps32, PfVps60 and PfBro1 did not recognize any structure in non-infected RBCs (S5A Fig). Neither the preimmune serum nor the secondary antibody controls displayed any signal in either RBC or pRBCs (S5B and S5C Fig).

PfVps32, PfVps60 and PfBro1 are present in extracellular vesicles produced by pRBCs

The results shown above suggested that ESCRT-III proteins could be involved in the export to the RBC cytoplasm of *Plasmodium*-derived proteins. To analyze whether ESCRT-III proteins were also present in EVs derived from pRBCs, we first evaluated by stochastic optical reconstruction microscopy (STORM) the presence of PfVps32, PfVps60 and PfBro1 in EVs derived from infected and non-infected RBCs. The higher resolution (~20 nm) of this technique compared to confocal microscopy (~0.5 μm), together with its high sensitivity, allowed us to precisely localize individual proteins in single EVs, whose size varies between 50 nm and 1 μm [9]. Parasite proteins were observed in EVs purified from a 3% parasitemia pRBC culture at 40 hpi (Fig 2A) and were absent in EVs from non-infected RBCs (Fig 2B), which confirmed

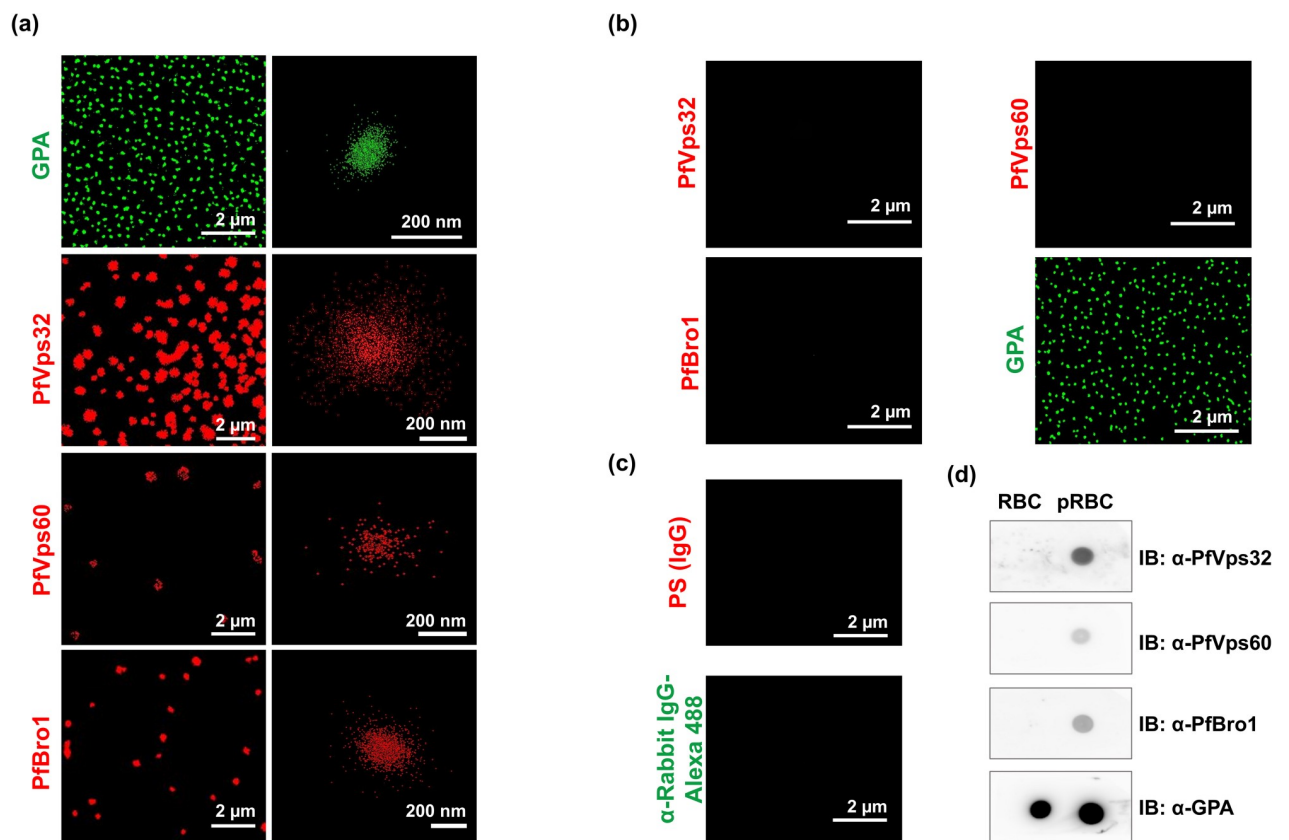


Fig 2. PfVps32, PfVps60 and PfBro1 proteins are present in EVs produced by pRBCs. (a) STORM detection by immunostaining of GPA, PfVps32, PfVps60 or PfBro1 in purified EVs derived from a 3% parasitemia, 3% hematocrit pRBC culture at 40 hpi. On the right column are shown images of individual EVs. (b) STORM detection as in (a) but using EVs derived from a 3% hematocrit RBC culture incubated for 40 h at 37°C. (c) Control of pRBC-derived EVs immunostained with preimmune serum (PS) or secondary antibodies against rabbit IgGs. (d) Dot blot assays performed in extracts of EVs derived from pRBCs (at 40 hpi) and RBCs (after 40 h of incubation at 37°C).

<https://doi.org/10.1371/journal.ppat.1009455.g002>

our hypothesis and reflected ESCRT-III participation in *Plasmodium* EV biogenesis. To validate our approach, antibodies against GPA were used to detect EVs from RBC membrane origin (Fig 2A and 2B). Incubation of EVs derived from pRBCs with preimmune serum or secondary antibodies did not detect any signal (Fig 2C). STORM detection was confirmed by dot blot assays using proteins extracted from RBC- and pRBC-derived EVs. In this case, PfVps32, PfVps60 and PfBro1 were only detected in extracts from pRBC-EVs. As expected, control GPA was detected in EVs derived from both RBCs and pRBCs (Fig 2D).

PfBro1 binds to membranes and recruits both PfVps32 and PfVps60 to trigger bud formation

So far, our results strongly suggested that there is a minimal ESCRT-III machinery participating in the formation of EVs in *P. falciparum*. Due to the fast binding and action of ESCRT-III proteins, it is difficult to assess their function in living cells. Other ESCRT-III mechanisms have been studied with the giant unilamellar vesicle (GUV) membrane model [33,34], which allows control of the lipid composition and visualization of the effects of ESCRT-III proteins on membranes by fluorescence microscopy.

To investigate whether *P. falciparum* ESCRT-III-related proteins were able to trigger membrane deformations, GUVs composed by palmitoyl-oleoyl-phosphatidylcholine (POPC) and palmitoyl-oleoyl-phosphatidylserine (POPS) (80:20) were generated to mimic the composition of the inner leaflet from the RBC plasma membrane [35]. We also included the fluorophore 1, 1'-dioctadecyl-3,3,3',3'-tetramethylindocarbocyanine perchlorate (DiI_{C18}) to visualize membrane alterations (see [Materials and Methods](#)).

First, we tested the ability of PfBro1 to insert into lipid bilayers using its predicted hydrophobic sequence. When 600 nM of recombinant PfBro1 labeled with Oregon Green 488 (PfBro1-OG488) were incubated with POPC:POPS (80:20) GUVs diluted in an appropriate buffer, the protein inserted into GUV membranes with a homogenous distribution (Fig 3A). A truncated PfBro1 version lacking its hydrophobic domain (PfBro1t) failed to insert into GUV membranes (S6 Fig). Incubation in 150 mM NaCl, 25 mM tris-HCl, pH 7.4 (protein buffer) did not affect the GUV morphology (Fig 3A, top panel). After confirming PfBro1 binding to lipid bilayers, we investigated its role as a potential recruiter and activator of ESCRT-III proteins, in particular of Snf7-containing proteins. When POPC:POPS (80:20) GUVs were incubated with 600 nM of unlabeled PfBro1, followed by the addition of 1200 nM of either PfVps32 or PfVps60 labeled with Oregon green, the combination of both proteins induced the formation of intraluminal buds in the GUVs model (Fig 3B–3D). PfBro1+PfVps32-derived buds were significantly larger ($1.43 \pm 0.51 \mu\text{m}$) than those formed by PfBro1+PfVps60 ($1.23 \pm 0.52 \mu\text{m}$) (Fig 3d). Overall, these two bud types were smaller and more homogeneous in comparison to those where only PfBro1 was present (Fig 3D). Remarkably, the buds formed by PfBro1+PfVps60 exhibited a necklace-like arrangement and some tubular structures could be observed (see [S1 Video](#)). It is important to mention that the overall osmolarity of the mixture did not differ significantly after protein+buffer addition (~ 5 mOsmol/Kg change). As the incubation of GUVs with PfVps32 or PfVps60 only, either label-free or tagged with OG488, did not produce any detectable membrane changes (Fig 3B and 3C), we concluded that PfBro1 binds and activates both proteins.

Putative activation of PfVps60 by PfBro1

It is well known that the activation of ESCRT-III subunits occurs after the displacement of the C-terminal domain that is blocking the binding site in the inhibited form of the protein [36]. The rearrangement of this domain has been documented to occur upon binding of activation

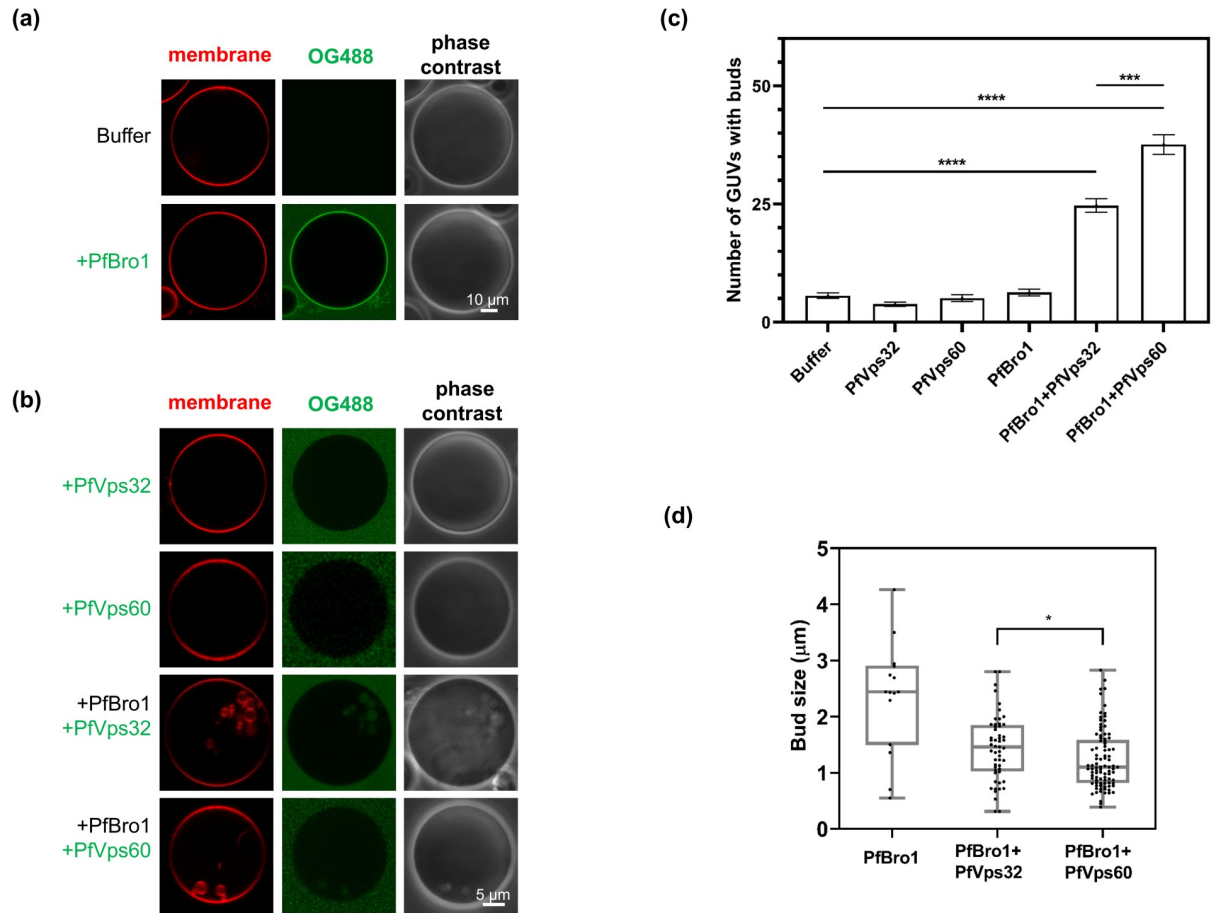


Fig 3. Intraluminal bud formation triggered by ESCRT-III *Plasmodium* proteins. GUVs composed by POPC:POPS (80:20), labeled with DiI_{C18} and diluted 1:2 in 2× protein buffer were incubated with (a) 600 nM PfBro1-OG488 with a 1:3 ratio of labeled and unlabeled protein, or (b) 1200 nM of either PfVps32 or PfVps60 labeled with OG488 (1:3 labeled:unlabeled) alone or in combination with 600 nM PfBro1 and visualized by fluorescence confocal microscopy. (c) Quantification of the number of GUVs with internal buds formed after protein addition. (d) Size of buds formed after the addition of the proteins indicated. Bars represent the mean and standard error of three independent experiments where 50 GUVs of each replicate were observed. *p* values were determined by Student's *t*-test. *: *p* < 0.05, ***: *p* < 0.001, ****: *p* < 0.0001.

<https://doi.org/10.1371/journal.ppat.1009455.g003>

factors such as Vps20, Vps32 or Bro1 [37]. To check whether this mechanism could be also operating in *P. falciparum*, we performed an *in silico* docking assay using the predicted tertiary structure of the Bro1 domain from PfBro1 and the full-length PfVps60 protein (see S1 Supporting Material and Methods for a full description of the methodology). This pair of proteins was selected because a higher number of GUVs with intraluminal buds was observed for this combination (Fig 3C). Upon binding to the PfBro1 domain, it was predicted that PfVps60 changed from a “closed” to an “open” conformation where the C-terminal domain modified its angle and allowed the exposure of the binding site (S7 Fig).

On the other hand, the colocalization of individual PfBro1 and PfVps60 molecules in pRBCs was further interrogated by STORM, taking advantage of the high sensitivity that this technique offers. Manders' overlap coefficient demonstrated that PfBro1 and PfVps60 colocalized in the trophozoite stage of the intraerythrocytic cycle (Fig 4A). Interestingly, vesicles labeled with PfBro1 and PfVps60 were detected bound to the surface of non-infected RBCs (Fig 4B). Immunoprecipitation assays using anti-PfBro1 antibodies as bait confirmed the

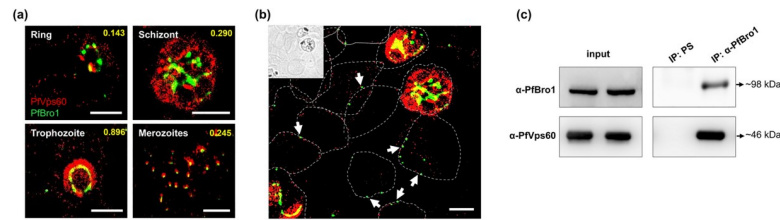


Fig 4. Interaction between PfVps60 and PfBro1. (a) STORM immunostaining detection of PfVps60 and PfBro1 in the blood stages of *P. falciparum*. (b) Field showing non-infected and infected RBCs. The inset contains a bright field low-resolution image to show the non-infected RBCs. Arrows pinpoint extracellular vesicles bound to non-infected RBCs, whose contours are indicated by dashed lines. Scale bars: 2 μ m. (c) Immunoprecipitation of pRBC lysates at 30 hpi using anti-PfBro1 antibodies or preimmune serum (PS).

<https://doi.org/10.1371/journal.ppat.1009455.g004>

association of PfBro1 with PfVps60 in the trophozoite stage (Fig 4C). Altogether, these results indicated that PfBro1 is able to bind and activate PfVps60.

PfBro1 and PfVps32 trigger bud formation by direct shedding from the plasma membrane

Using the purified recombinant proteins from *P. falciparum* and the GUV model we were able to reconstitute one of the two EV biogenesis pathways described in higher eukaryotic cells (MVB biogenesis; see review in [38]). However, the mechanism of microvesicle formation by direct shedding from the plasma membrane could not be reconstituted using this approach, and a microinjection strategy was designed for its study. For this, the biotinylated lipid 1,2-distearoyl-sn-glycero-3-phosphoethanolamine-N-[biotinyl(polyethylene glycol)-2000] (DSPE-PEG-biotin) was included in the lipid mixture to form GUVs containing protein buffer in their lumen (see Materials and Methods). GUVs were harvested and immobilized on an avidin-coated surface to allow their manipulation for injection. It is important to mention that prior to injection, a z-stack acquisition was performed in the confocal microscope to verify that GUVs lacked alterations in the membrane and that the contact area with the coverslip was not excessively large, which could compromise the assay (see example of a selected GUV in S8 Fig). As the labeling of proteins can compromise their activity, we used free polyethylene glycol fluorescein isothiocyanate (PEG-FITC) dye (0.03 mg/ml in protein buffer) to visualize the injection process. The incorporation of this control dye did not produce any detectable alterations in GUVs (see Figs 5 and S9, S2 Video). Upon injection of either PfBro1, PfVps32 or PfVps60 alone, or a combination of PfBro1 and PfVps60, no significant changes were observed in the membrane of the injected GUVs (Fig 5B). On the other hand, when PfBro1 and PfVps32 were injected together, the formation of extracellular buds was visualized in all the injected GUVs (Fig 5 and S3 Video). Contrary to the experiments observed in the previous approach (Fig 3), these buds appeared as single bodies with a homogeneous average size of $0.88 \pm 0.076 \mu$ m, and remained attached to the mother vesicle moving along its surface (S3 Video).

Disruption of PfVps60 causes a defect in EV production in *P. falciparum*

Next, we evaluated the effect of ESCRT-III machinery inactivation on EV production by *P. falciparum*. While we failed at obtaining a stable strain for the KO of *PfVps32* and *PfBro1* (probably due to their essential role in the life cycle of the parasite), we succeeded in the establishment of a *PfVps60* KO strain by CRISPR/Cas9 gene edition (Fig 6A). Gene silencing and DNA integration were confirmed by diagnostic PCR as shown in Fig 6B. The relative

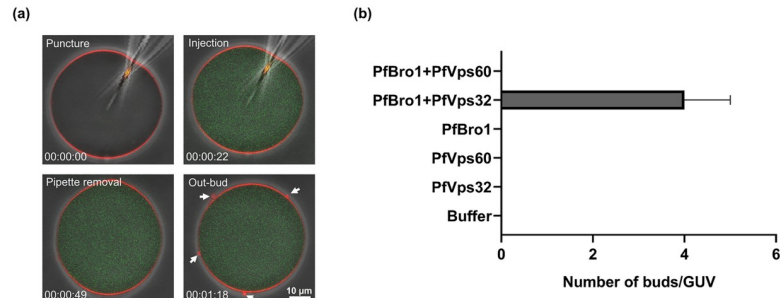


Fig 5. Injection of ESCRT-III *Plasmodium* proteins in GUVs and outward budding. (a) Panels show injection of a mixture of PfBro1 and PfVps32 (1:2) together with PEG-FITC in GUVs composed by POPC:POPS:DSPE-biotin (79:20:1) and labeled with DiI_{C18} (0.1 mol%). Four main events are presented: puncture, injection, pipette removal and generation of outward buds (arrows). (b) Graphical representation of bud number per GUV in the tested conditions for the injection approach. Bars represent the mean and standard error of the number of out-buds in four independent injected GUVs.

<https://doi.org/10.1371/journal.ppat.1009455.g005>

fitness of the generated KO line was evaluated by a growth curve, which showed a slower progression in the KO line compared to its parental line (intraerythrocytic developmental cycle of 52.38 vs. 55.41 h, respectively; Fig 6C). The suppression of PfVps60 was confirmed by immunofluorescence assays, which indicated the absence of the protein (Fig 6D). In order to study the effects of the *PfVps60* gene disruption on EV production, EVs derived from WT and KO strains were purified in parallel and following the same protocol (see Materials and Methods). The resulting EV fractions were concentrated and resuspended to the same volume, and the amount of EV particles was determined. The number of EVs was significantly reduced in KO parasites in comparison to the parental 3D7 line (Fig 6E). Moreover, the measurements of

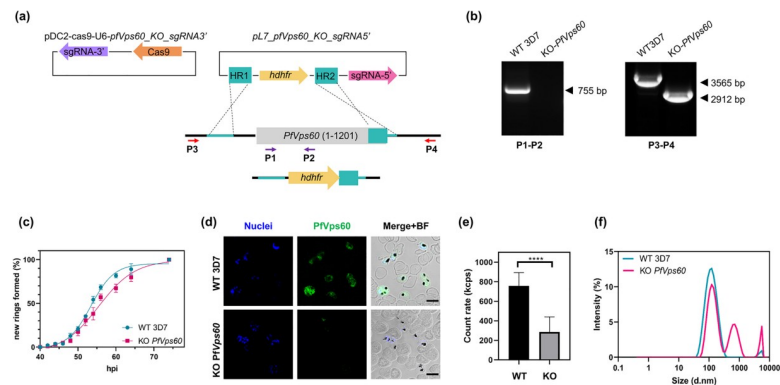


Fig 6. Generation and validation of *PfVps60* KO parasites. (a) Scheme of the strategy followed to generate the transgenic lines using the CRISPR/Cas9 system. Arrows indicate the position of primers used for diagnostic PCR. (b) Diagnostic PCR confirmation of the integration of the pL7-*PfVps60*_KO_sgRNA3' plasmid at the *PfVps60* locus. Legends at the bottom of each panel indicate the primer pair used for each PCR reaction. Genomic DNA from the WT 3D7 line or the *PfVps60* KO transgenic line was used. The expected size of the bands is indicated on the right side of each panel. (c) Asexual blood cycle duration in the *PfVps60* KO line compared with its parental 3D7 line. Percentages indicate the proportion of rings observed relative to the total number of rings at the end of the assay. Data was fitted to a sigmoidal curve with variable slope to extract the intraerythrocytic developmental cycle. (d) Human erythrocytes infected with *P. falciparum* were fixed and PfVps60 (green) was detected by indirect immunofluorescence microscopy. Cell nuclei were visualized with Hoechst 33342 (blue). Fields were merged with bright field (BF) to assess localization. Scale bar: 5 μm. (e) Derived count rate of purified EVs from three independent replicates expressed in kilo counts per second (kcps). (f) Representative results of the size distribution of EVs derived from the WT 3D7 or the KO *PfVps60* strains determined using a Zetasizer Nano. Each symbol shows the mean of three different replicates, bars show the SE. ***: *p* < 0.0001.

<https://doi.org/10.1371/journal.ppat.1009455.g006>

particle size showed that the distribution of EVs differed between the KO and WT strains. In the WT, there were two main populations, one with a diameter of 40–300 nm and the other between 3–5 μm . In the KO, three populations with different diameters were revealed: 60–300 nm, 300–1,000 nm and 4,000–5,000 nm (Fig 6F).

To assess whether the observed EV reduction was only due to the effect of PfVps60 absence or to a generalized disruption of the ESCRT machinery, we evaluated the distribution of PfVps32 and PfBro1 in the KO line. As shown in Fig 7A, both proteins appeared clustered around the periphery of the parasite, and in some cases large vesicular-like structures stained with PfBro1 were observed (Fig 7A, arrowhead). However, some PfVps32- and PfBro1-labeled puncta were observed adjacent to the RBC plasma membrane suggesting their export to the RBC cytoplasmic space. To confirm this, Western blot assays performed in total protein extracts 40 hpi revealed that the total amount of PfVps32 and PfBro1 remained unaltered in the KO strain (Fig 7B). However, we could observe a partial drop in the level of both proteins present in the saponin fraction, which confirmed that the proteins were still exported outside the PV but in lower amounts (Fig 7B).

Discussion

Throughout its intraerythrocytic life cycle, *Plasmodium* resides within a PV where it needs to overcome the scarcity of nutrients and the absence of an exploitable cell machinery in the mature RBC. As a result, *Plasmodium* has evolved specialized and complex trafficking pathways, which allow the export of virulence-related proteins to the RBC cytoplasm or to the extracellular space [39]. Most of the exported proteins contain an N-terminal PEXEL motif and are carried outside the PV through a protein translocon inserted in the PV membrane [40]. However, other routes allow the transport of non-PEXEL proteins [41]. Among them, the secretory vesicle pathway that has been poorly investigated despite its participation in the transport of crucial proteins for the pathophysiology of the disease and in the transfer of drug resistance genes [42,43].

Plasmodium-infected erythrocytes increase the release of EVs, which participate in different pathogenic mechanisms (see review in [44]). Some proteins related with EV biogenesis have been elucidated, such as PfPTP2, which is involved in the intercellular communication between *P. falciparum* infected cells and that has been identified in vesicles in close contact with parasite-derived membranous structures present in the RBC cytoplasm, called Maurer's clefts [43]. In higher eukaryotes, the ESCRT-III machinery is involved in both types of EV generation: exosome release and microvesicle budding [45,46]. However, the mechanisms underlying the release of EVs in *Plasmodium*-infected cells are far from being understood. The *P. falciparum* genome lacks genes encoding for ESCRT-III activating factors, such as Vps20 and ESCRT-II members [27]. Therefore, we hypothesize that there are alternative pathways for ESCRT-III activation in *P. falciparum* and most likely in other intracellular protists such as *T. gondii* and *Cryptosporidium parvum*, which also lack the aforementioned genes [23]. In *S. cerevisiae* and humans, Bro1 homologues are able to bind directly to the Snf7 domain of Vps32 and CHMP5 (Vps60 homologue) and activate ESCRT-III polymerization on the membranes [24,30,47]. In the present study, we show that *P. falciparum* possesses a Bro1 domain-containing protein, PfBro1, capable of activating two Snf7-domain containing proteins, PfVps32 and PfVps60, to trigger the formation of buds in the model of GUVs. These proteins are expressed throughout the intraerythrocytic cycle and are localized in the cytoplasm of the parasite inside the PV. However, PfVps32 and PfBro1 are also exported to the cytoplasm of the RBC, where they can participate in the biogenesis of microvesicles through plasma membrane shedding as discussed below. The identified PfBro1 has a hydrophobic sequence in its C-terminal region

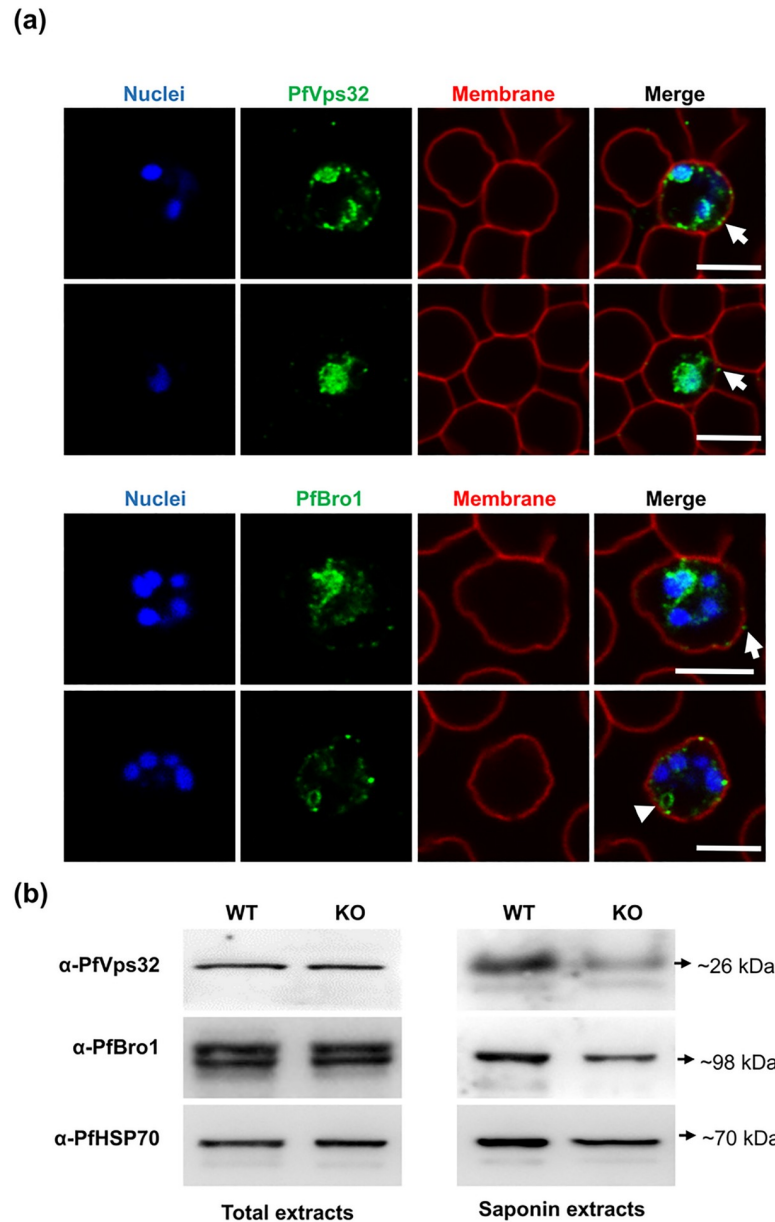


Fig 7. Effect on PfVps32 and PfBro1 by PfVps60 disruption. (a) Representative images of human erythrocytes infected with a *P. falciparum* KO-*PfVps60* strain and fixed with 4% PFA to detect PfVps32 and PfBro1 proteins (green) and WGA (red) by indirect immunofluorescence. Cell nuclei were visualized with Hoechst 33342 (blue). Arrows show protein-labeled puncta adjacent to the membrane of the pRBCs. The arrowhead shows a vesicle-like structure labeled with PfBro1. For each protein are shown two microscope fields corresponding to the KO strain. Scale bars: 10 μ m. (b) Western blot assays using total protein extracts or the saponin fraction obtained from pRBCs infected with either the WT 3D7 or the KO-*PfVps60* strain to detect proteins indicated on the left side of the panels.

<https://doi.org/10.1371/journal.ppat.1009455.g007>

that allows its insertion into GUV lipid bilayers, thus making it a good candidate for ESCRT-III recruitment at the membrane. Moreover, we have also identified a conserved PEXEL motif in its N-terminal region (RNLKE) which could be involved in facilitating the export of PfBro1 from the PV to the RBC cytoplasm as already described for other PEXEL-containing proteins [48], however, more experiments are required to confirm this. On the contrary,

PfVps32 and PfVps60 lack a PEXEL motif, which suggest that their export is carried out through a different mechanism.

The study of ESCRT-III interactions in living cells is problematic as the association between the different molecular components occurs in a fast manner and the protein complexes are difficult to obtain. Therefore, *in silico* docking assays were performed and the results showed that PfVps60 can shift from a closed (inactive) to an open (active) conformation upon PfBro1 interaction. This association was confirmed by STORM imaging and immunoprecipitation assays. Furthermore, we proved that PfBro1 is able to recruit both PfVps32 and PfVps60 to the GUV membrane and activate them, leading to the formation of buds, as occurs in the same model with other ESCRT-III homologues [34,49]. The purified proteins were used to recreate the two mechanisms of EV production (MVB generation and membrane shedding) in GUVs that mimic the composition of the inner leaflet of the erythrocyte plasma membrane. Interestingly, while bud generation is triggered by both PfVps32 and PfVps60 in a similar manner when the proteins are added outside the GUV, in the injection approach, we observed that bud formation was triggered only by the co-injection of PfBro1 and PfVps32. This discrepancy might be due to the requirement for a higher concentration of PfVps60 to drive membrane deformation, which cannot be achieved in the GUV femtoinjection approach. The presence of PfVps60 in the PV lumen would therefore suggest that the protein is present in sufficiently high amounts to allow its participation in MVBs formation inside the PV (Fig 8A) and in the budding of MVBs from the PV membrane (Fig 8B), both processes leading to exosome export. In GUV injection assays, PfVps32 was able to trigger bud formation at a fixed PfBro1 concentration, which reflects the efficiency of this protein to polymerize and deform membranes at low concentration. This scenario would not require that large amounts of PfVps32 are exported to the RBC plasma membrane for it to participate in the budding of microvesicles (Fig 8C).

We also observed that when the addition of PfVps32 or PfVps60 led to bud formation, the nascent vesicles varied in size depending on the protein used, with PfVps32 leading to significantly bigger buds in comparison to PfVps60. In higher eukaryotes there are several factors governing the size of ESCRT-III-derived buds, including Vps4 disassembly action [50,51], size of cargo [34] and membrane tension [49]. In the case of *P. falciparum*, whether the size of EVs is regulated by other ESCRT proteins encoded in its genome or by membrane biophysical properties, remains to be explored in the future. On the other hand, as the newly formed buds remained in close contact with the mother vesicle, we hypothesize that more factors are needed to release the nascent vesicle from the membrane.

The detection of PfBro1, PfVps32 and PfVps60 in purified EVs from a pRBC culture suggests that the ESCRT-III machinery participates in their biogenesis. Furthermore, silencing of the *PfVps60* gene resulted in the reduction of the number of EVs produced during the first 40 hpi, which indicates the participation of PfVps60 in EV biogenesis during *Plasmodium* infection. Although our initial aim was to inactivate the whole ESCRT-III complex, we could not obtain stable KO lines for PfVps32 and PfBro1 proteins, probably due to their involvement in essential processes from the parasite, most likely in cytokinesis as occurs in other eukaryotes [50,52]. The increase in the microvesicle population (<300 nm) observed in the KO strain could reflect that either other EV-production mechanisms in *P. falciparum* are enhanced or an alteration in the export mechanisms is produced upon *PfVps60* silencing. On the other hand, the subcellular distribution of PfVps32 and PfBro1 changed significantly with the disruption of the *PfVps60* gene. Both proteins were clustered around the periphery of the parasite, although their export to the RBC cytoplasm was conserved but in a reduced degree. It has been demonstrated that the depletion of *Vps* genes in other organisms resulted in mislocalization of MVB cargoes to the limiting membrane of the vacuole or to large aberrant structures called class E compartments [53,54]. STORM imaging allowed us to detect EVs labeled with PfBro1

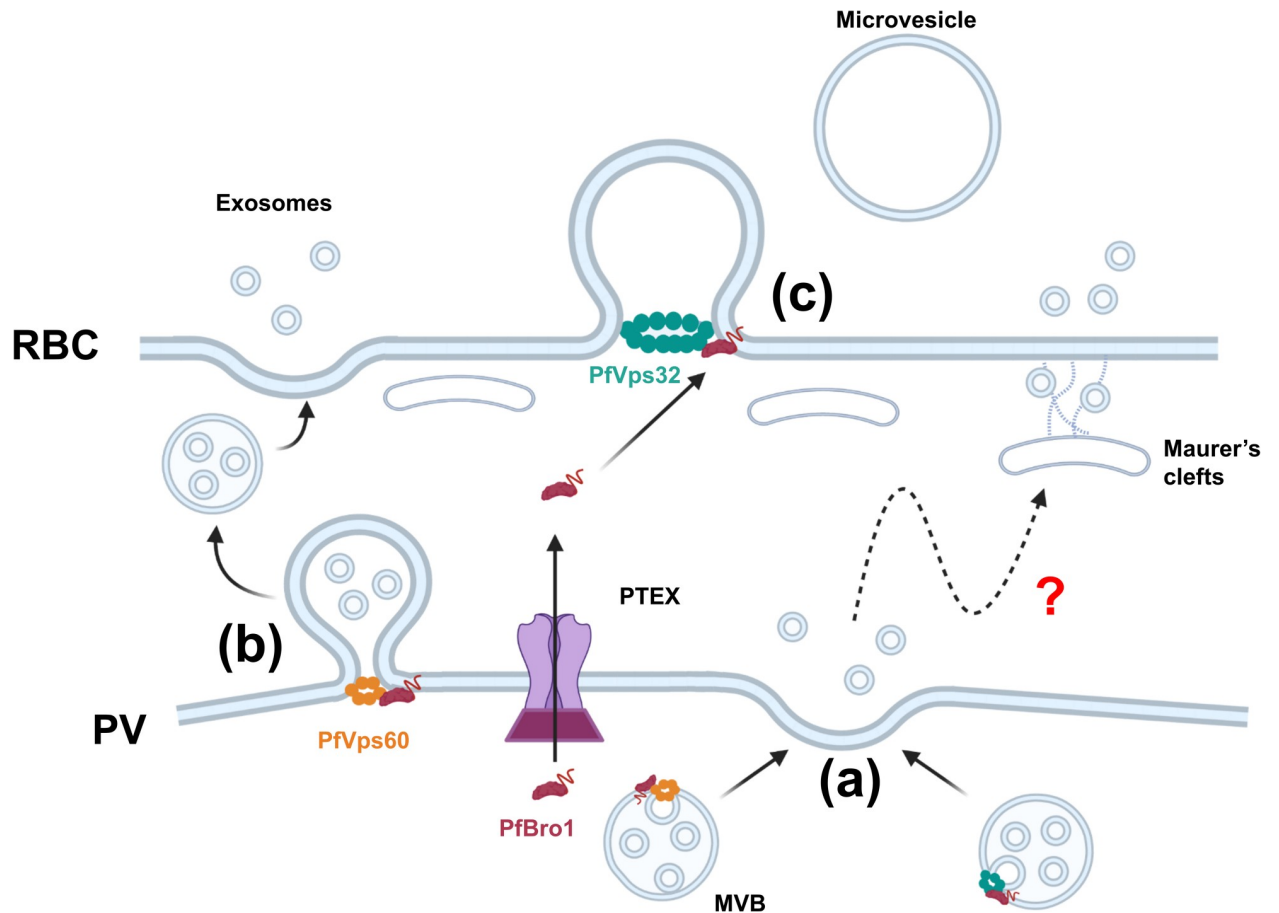


Fig 8. Proposed model for ESCRT-III-mediated EV biogenesis in *Plasmodium*. (a) PfVps32 and PfVps60 are recruited by PfBro1 and trigger the formation of intraluminal vesicles (ILVs) to generate MVBs. These MVBs fuse with the parasitophorous vacuole (PV) membrane and release the ILVs into the host cytoplasm through which they can be transported via the exo-membranous trafficking system present in pRBCs to be eventually released to the extracellular space. (b) MVBs are formed directly in the PV membrane after the insertion of PfBro1 which recruits PfVps60, generating MVBs that are released to the host cytoplasm. These MVBs eventually fuse with the RBC plasma membrane to release exosomes to the extracellular space. (c) PfBro1 can also be exported from the PV to the host cell through the PTEX. Once in the host cytoplasm, PfBro1 can insert into the RBC plasma membrane and recruit PfVps32 (which is exported by an as yet unknown mechanism) to initiate budding and trigger microvesicle formation. Created with [BioRender.com](https://www.biorender.com).

<https://doi.org/10.1371/journal.ppat.1009455.g008>

and PfVps60 at the surface of non-infected erythrocytes, thus suggesting their involvement in a potential pathogenic priming mechanism that could facilitate invasion of targeted cells.

In conclusion, we propose that the mechanism of ESCRT-III-mediated EV biogenesis in *Plasmodium* starts at the PV lumen. In here, PfVps60 and PfBro1 might trigger the formation of MVBs where proteins destined for export are sorted in the intraluminal vesicles (ILVs). The release of ILVs can possibly occur by two different mechanisms: (1) MVBs formed in the PV lumen fuse with the PV membrane (PVM) and release the ILV into the host cytoplasm where they can be transported to the RBC plasma membrane via the exo-membranous trafficking system present in pRBCs (Fig 8A, see review in [55]), or (2) MVBs are formed directly in the PVM after the insertion of PfBro1, generating MVBs that are released to the host cytoplasm which latter fuse with the RBC plasma membrane to release exosomes to the extracellular space (Fig 8B). On the other hand, PfBro1 can also be exported from the PV to the host cell through the *Plasmodium* translocon of exported proteins (PTEX). Once in the host cytoplasm, PfBro1 can insert into the RBC plasma membrane and recruit PfVps32 (which is exported by

an as yet unknown mechanism) to initiate budding and trigger microvesicle formation (Fig 8C).

Altogether, these results strongly suggest that both types of EV formation are being carried out in *Plasmodium*-infected RBCs, thus supporting previous observations [43,56]. Our results improve the mechanistic understanding of protein export in *P. falciparum*, and suggest that the proteins studied here represent a potential target for new therapeutic strategies to control malaria.

Materials and methods

More information is available in the Supporting Materials and Methods.

P. falciparum culture and synchronization

Unless otherwise indicated, reagents were purchased from Sigma-Aldrich (St. Louis, MO, USA). Asexual stages of *P. falciparum* 3D7 were propagated in group B human erythrocytes at 3% hematocrit using Roswell Park Memorial Institute (RPMI) medium supplemented with 0.5% (w/v) Albumax II (Life Technology, Auckland, New Zealand) and 2 mM L-glutamine. Parasites were maintained at 37°C under an atmosphere of 5% O₂, 5% CO₂ and 90% N₂. For all experiments, the parasitemia of the culture was kept between 3 and 5%.

For tight synchronization, the parasite culture was initially synchronized in the ring stage with a 5% sorbitol lysis [57] followed by a second 5% sorbitol lysis after 36 h. Then, 36 h after the second sorbitol, parasites were synchronized in the schizont stages by treatment in 70% Percoll (GE Healthcare, Uppsala, Sweden) density centrifugation at 1,070 × g for 10 min. Finally, after the third synchronization a final 5% sorbitol lysis was done, yielding parasites tightly synchronized at 8 hpi.

STORM

A 5% parasitemia RBC culture was prepared for super-resolution microscopy as described in [58]. Briefly, a μ-Slide 8 well chamber slide (Ibidi) was coated for 20 min at 37°C with 50 mg/ml concanavalin A. Then, wells were rinsed with pre-warmed phosphate buffered saline (PBS) before parasite seeding. Infected RBCs were washed twice with PBS and deposited into the wells. Cells were incubated for 10 min at 37°C and unbound RBCs were washed away with three PBS rinses. Seeded RBCs were fixed with pre-warmed 4% paraformaldehyde at 37°C for 20 min. After this time, cells were washed with PBS and then, incubated with polyclonal antibodies anti-PfVps60-Alexa Fluor 488 (1:500) and anti-PfBro1-Alexa Fluor 647 (1:1000). Finally, nuclei were counterstained with Hoechst 33342 (2 μg/ml).

Before STORM acquisition, the buffer was exchanged to OxEA buffer (3% v/v oxyrase, 100 μM DL-lactate, 100 mM β-mercaptoethylamine, dissolved in 1× PBS, pH 8.4) [59]. STORM images were acquired using a Nikon N-STORM system configured for total internal reflection fluorescence imaging. Excitation inclination was tuned to adjust focus and to maximize the signal-to-noise ratio. Alexa Fluor 647 and 488 were excited, respectively, illuminating the sample with 647 nm and 488 nm laser lines built into the microscope. Fluorescence was collected by means of a Nikon 100×, 1.4 NA oil immersion objective and passed through a quad-band-pass dichroic filter (97335 Nikon). 20,000 frames at 50 Hz were acquired for each channel. Images were recorded onto a 256×256 pixel region (pixel size 160 nm) of a CMOS camera. STORM images were analyzed with the STORM module of the NIS element Nikon software.

Reconstitution of ESCRT-III in GUVs

GUVs containing POPC, POPS, and the fluorophore DiI_{C18} (Invitrogen, CA, USA) (80:20:0.1) were prepared in 600 mM sucrose as described previously [33]. Briefly, the lipid mix was spread on tin oxide-coated glass slides, and electro-swelling was performed for 1 h at room temperature (RT) at 1.2 V, and 10 Hz. All lipids were obtained from Avanti Polar Lipids (Alabaster, IL, USA).

For PfBro1 binding assays, GUVs were harvested and diluted 1:1 with 2× protein buffer (50 mM tris-HCl, 300 mM NaCl, pH 7.4). After 10 min of equilibration, GUVs were incubated with 600 nM of either PfBro1- or PfBro1t-OG488. For PfVps recruitment, equilibrated GUVs were incubated with 600 nM of PfBro1 and 1200 nM of either PfVps32 or PfVps60 with at least 10 min of incubation at RT between the additions of each protein. Images were acquired with a Leica TCS SP5 confocal microscope (Mannheim, Germany). DiI_{C18} was excited with a 561 nm laser and OG488 with a 488 nm line of an Argon laser. To avoid crosstalk between the different fluorescence signals, a sequential scanning was performed. All experiments shown in the same figure were done with the same GUV batch for comparability. Each experiment was repeated on at least three separate occasions with different batches of GUVs.

Femtoliter injection

A lipid mixture of POPC, POPS, DSPE-PEG-biotin, and 1,2-dipalmitoyl-sn-glycero-3-phosphoethanolamine (DPPE)-rhodamine (78.9:20:1:0.1 mol%) was prepared in chloroform. GUVs filled with protein buffer were grown by the gel-assisted method [60]. Briefly, a 5% (w/w) polyvinyl alcohol (PVA) solution was prepared in protein buffer (25 mM tris-HCl, pH 7.4, 150 mM NaCl). The PVA solution was spread on a microscope coverslip and then dried for at least 30 min at 50°C. 10–15 µl of lipids dissolved in chloroform (1 mg/ml) were spread on the dried PVA film and placed under vacuum for 1 h to eliminate the solvent. A chamber was formed with a homemade Teflon spacer sandwiched between two microscope slides and filled with protein buffer for 10 min at RT. Then, GUVs were harvested by gentle tapping on the bottom of the chamber and collected using a micropipette without touching the PVA film to avoid sample contamination. To immobilize GUVs, cleaned coverslips were incubated for 20 min at RT with a 1:1 mixture of 1 mg/ml BSA-biotin and 1 mg/ml BSA (both diluted in protein buffer to maintain osmolarity), following the protocol from [61]. After incubation, coverslips were washed with distilled water and incubated with 0.005 mg/ml avidin. Subsequently, slides were washed and dried with N₂. These coverslips were used to assemble a homemade observation chamber using a Teflon spacer, where GUVs were deposited and let to settle down for at least 10 min.

The micropipettes used to perform the injection were fabricated from thin wall borosilicate glass capillaries with filament (Harvard Apparatus, Holliston, MA, USA) in a pipette puller (Sutter Instruments, Novato, CA, USA) to obtain bee-needle type tips. For the injection experiments, immobilized GUVs were imaged under a Leica TCS SP5 confocal microscope. The micropipette was placed on a mechanical holder attached to a micromanipulator (Sutter Instruments) and then connected to a Femtojet microinjector set (Eppendorf). Injection was performed in a 15° angle, using a pressure of injection of 150 hPa, time of injection of 5.0 s and a compensation pressure of 1 hPa. The solution injected corresponded to a 4× protein mixture stock (2.4 mM PfBro1 and 4.8 mM of either PfVps32 or PfVps60 dissolved in 1× buffer) or its individual components, and 0.03 mg/ml PEG-FITC to monitor injection.

Generation of *PfVps60* KO strain

Homology regions (HR) of the 5'UTR (HR1, spanning positions –762 to –243 from the *PfVps60* start codon) and 3'UTR (HR2, spanning positions 1,012 to 1,553 from the *PfVps60*

start codon) were PCR amplified using genomic DNA purified from a *P. falciparum* 3D7 culture synchronized at late stages. Primers used for PCR amplification are listed in S2 table. The generated HR1 and HR2 were cloned by ligation using restriction sites *SpeI* and *AflIII* (HR1), and *EcoRI* and *NcoI* (HR2) into a modified pL6-*egfp* donor plasmid [62] in which the *yfcu* cassette had been removed [63]. The single guide RNA (sgRNA) specific for the *PfVps60* gene and targeting the sequence near the 5' end (sgRNA 5', position -225, -206) was generated by cloning annealed oligonucleotides into the *BtgZI* site to generate the pL7-*pfvps60_KO_sgRNA5'* plasmid. On the other hand, the pDC2-Cas9-U6-*hdhfr* vector [64] was modified by cloning a sgRNA specific for the sequence near the 3' end (sgRNA 3', position 980, 999) into the *BtgZI* site of this plasmid to generate the pDC2-Cas9-U6-*pfvps60_KO_sgRNA3'* plasmid. All guides were cloned using the In-Fusion system (Clontech, Japan).

For transfection of 3D7 rings, 60 μ g of circular pDC2-Cas9-U6-*hdhfr-pfvps60_KO_sgRNA3'* plasmid and 30 μ g of linearized (with *PvuI*) donor plasmid were precipitated, washed and resuspended in 30 μ l of sterile 10 mM Tris, 1 mM EDTA (TE) buffer. Then, plasmids were diluted in 370 μ l of Cytomix buffer (120 mM KCl, 0.15 mM CaCl₂, 10 mM K₂HPO₄/KH₂PO₄, 25 mM Hepes, 2 mM EGTA, 5 mM MgCl₂, pH 7.6) and introduced into parasites by electroporation using a Bio-Rad Gene Pulser Xcell system, at 310 V, 950 μ F of capacitance and without resistance. Electroporated parasites were carefully recovered and resuspended in RPMI medium supplemented with 0.5% (w/v) Albumax II and 2 mM L-glutamine. Twenty-four hours after transfection, cultures were selected with 10 nM WR99210 for 4 consecutive days [65]. To validate the integration of the plasmids, a diagnostic PCR analysis was performed using LA Taq DNA polymerase (Takara, Japan), the primers listed in S2 Table and gDNA obtained from the *PfVps60* KO strain, and compared with the WT 3D7 strain. The fitness of the generated line, compared with the parental 3D7 line, was evaluated by calculating the percentage of newly formed rings in tightly synchronized cultures. Initial parasitemia was determined at ~18 hpi, then rings parasitemia was determined at different time points within the period where most schizont bursting and reinvasion events occurred (44 to 62 hpi). The final point was 74 hpi when all viable schizonts had burst. Data points were determined by the proportion of rings relative to the total number of rings at the end of the assay. Data was fitted to a sigmoidal dose-response curve and the time to generate 50% or the rings in each population was determined [66].

EVs purification

For purification of EVs, medium was collected at 40 hpi from pRBC cultures with an initial parasitemia of 3%. EV isolation was performed as previously described [67]. Briefly, samples were prepared by sequential centrifugations of conditioned medium to remove large aggregates. First, cultures were centrifuged for 10 min at 400 \times g, the cell pellet was discarded, and supernatant was further centrifuged at 2,000 \times g for 10 min twice. In both cases, a small pellet was discarded. Finally, 25 ml of the supernatant was placed in an Amicon Ultra-15 centrifugal filter (100 kDa cut-off, Millipore-Merck, Cork, Ireland) and centrifuged for 20 min at 3,400 \times g. One ml of the resulting concentrated solution was collected and transferred to a 10 ml homemade Sepharose CL-4B column previously equilibrated with PBS. EV purification was performed by gravity flow at RT and 0.5-ml fractions were collected. EVs were enriched in fractions 8 and 9, which were combined, concentrated and resuspended to a final volume of 200 μ l to be used for the rest of EV characterization experiments.

EV size and abundance measurements

Dynamic light scattering was used to measure particle size in the purified EVs population as described before [68]. In order to obtain the optimum light scattering intensity, 100 μ l of

purified EVs were resuspended in 900 μ l of filtered (0.22 μ m) PBS diluted 1:2 in 4% paraformaldehyde (PFA). Mean particle size of vesicle dispersions and the derived count rate (Kilo counts per second, kcps) were determined in triplicates from light diffusion measured at 25°C and an attenuator index of 8, using Zetasizer Nano S (Malvern Instruments, Ltd., Malvern, UK).

EVs imaging

For STORM visualization of purified EVs, the protocol for super-resolution microscopy of vaccinia virus particles described by Gray & Albrecht [69] was followed. Briefly, a clean coverslip was washed 3 times with ethanol, acetone and deionized water sequentially. Then, coverslips were sonicated in 1 M KOH for 20 min at RT, washed thoroughly with water and placed in a 12-well plate. Next, the purified EVs were sonicated for 30 s to avoid aggregation, diluted in 1 mM tris-HCl, pH 9.0, and deposited on the cleaned coverslips. EVs were left to adhere for 60 min at RT and the rest of the solution was carefully removed with a pipette. The bound EVs were then fixed with 4% PFA for 15 min at RT, washed and incubated in quenching buffer (0.25% NH₄Cl in PBS) for 5 min at RT. After this time, EV-coated coverslips were incubated with blocking solution (5% BSA in PBS) for 30 min at RT and then, with either anti-PfVps32, anti-PfVps60 or anti-PfBro1 polyclonal antibodies labeled with Alexa Fluor 647 (1:100 in all cases) to detect EVs from parasite origin, or anti-GPA, (1:100), followed by anti-rabbit Alexa Fluor 488 (1:100), to reveal EVs derived from the RBC plasma membrane. Finally, coverslips were mounted with OxEA buffer for STORM imaging as described previously.

Supporting information

S1 Table. Snf-7 domain-containing proteins encoded in the *P. falciparum* genome. Modified from [23]. Percentages of similarity (S), identity (I) and expectation value (E-value) relative to *P. falciparum* proteins were determined using the Expert Protein Analysis Systems (ExPASy) Proteomics Server by the NCBI BLAST service program. (TIF)

S2 Table. Primers used for CRISPR/Cas9 gene edition. (TIF)

S1 Fig. Multiple sequence alignment for Bro1-homologues in yeast (Bro1), *P. falciparum* (PfBro1) and humans (Alix). Conserved residues are shadowed in blue. Conserved amino acids present in Bro1-containing proteins are indicated with colored circles, yellow for the polar cluster I and green for the polar cluster II. A key isoleucine involved in Vps32 binding is indicated with a star. The conserved PEXEL motif is double underlined in pink. The secondary structure for PfBro1 is displayed below the sequences, alpha helices represented in red and beta-sheets in green. Sequence alignments were performed with Clustal Omega and edited in Jalview 2. (TIF)

S2 Fig. Tertiary prediction and membrane orientation of PfBro1. The hydrophobic tail is colored in pink. Outer membrane leaflet is colored in red, inner leaflet in blue. The structure was generated using the Phyre2 server and the OPM database. (TIF)

S3 Fig. Purification of proteins and antibody validation. Left panels: SDS-PAGE gels stained with Coomassie blue showing the purified fractions of (a) PfVps32, (b) PfVps60 and (c) PfBro1 that were used for this study. The rest of the panels show Western blot assays of the

induced bacterial lysates (r) or *P. falciparum*-infected RBCs (*P.f.*) at 30 hours post invasion, using the specific antibodies or preimmune serum (PS) as indicated above the corresponding panels. Arrows indicate the approximate molecular weight. The polyacrylamide percentage is indicated below each gel.

(TIF)

S4 Fig. Expression of PfVps32, PfVps60 and PfBro1 during the *P. falciparum* intraerythrocytic cycle. Western blot analysis of *P. falciparum* in saponin, Triton X-100 or RIPA buffer protein extracts at different hours post invasion (indicated above the upper panels) to monitor protein expression of (a) PfVps32, (b) PfVps60 and (c) PfBro1. Arrows indicate the approximate molecular weight. IB: antibody used for loading control in the lower panels.

(TIF)

S5 Fig. Antibody validation for fluorescence confocal microscopy assays. Human erythrocytes were infected with *P. falciparum* and fixed with 4% PFA. (a) PfVps32, PfVps60 or PfBro1 (green) and WGA (red) were detected by indirect confocal immunofluorescence microscopy using the corresponding specific antibodies. Non-infected red blood cells did not show any antibody recognition. As negative controls, cells were incubated with (b) IgGs purified from preimmune serum (PS) or (c) only the secondary antibody anti-rabbit-Alexa488. Cell nuclei were visualized with Hoechst 33342 (blue). Scale bar: 10 μ m.

(TIF)

S6 Fig. Incubation of PfBro1t-OG488 with GUVs. POPC:POPS (80:20) GUVs labeled with DiI_{C18} were diluted in protein buffer, incubated with 600 nM of PfBro1t in a 1:3 ratio (labeled: unlabeled protein), and visualized by fluorescence confocal microscopy.

(TIF)

S7 Fig. Protein docking of PfBro1 and PfVps60. Predicted structure of (a) PfVps60 in its auto-inhibited form and (b) Bro1-domain of PfBro1. (c) Protein docking simulation showing the PfVps60 “opening”. All images were generated using PyMOL.

(TIF)

S8 Fig. Representative images of a GUV selected for injection. Panels show the top and side view of a typical vesicle selected to perform protein injection.

(TIF)

S9 Fig. Femtoliter injection of PEG-FITC in protein buffer. GUVs composed by POPC:POPS:DSPE-biotin (79:20:1) and labeled with DPPE-rhodamine (0.1 mol%) were grown on a PVA substrate using protein buffer, harvested after 10 min and deposited on an avidin-coated coverslip, and injected with PEG-FITC. No alterations were observed up to 5 min after injection.

(TIF)

S1 Video. Z-stack reconstruction by fluorescence confocal microscopy of POPC:POPS (80:20) GUVs labeled with DiI_{C18} (0.1 mol%) incubated with 600 nM PfBro1 and 1200 nM PfVps60. Intraluminal and interconnected buds of different sizes and some tubular structures are observed.

(AVI)

S2 Video. Time-lapse fluorescence confocal microscopy of the injection of POPC:POPS:DSPE-biotin (79:20:1) GUVs labeled with DPPE-rhodamine (0.1 mol%) with free PEG-FITC. The video is accelerated 4.5 \times .

(AVI)

S3 Video. Time-lapse fluorescence confocal microscopy of the injection of POPC:POPS: DSPE-biotin (79:20:1) GUVs labeled with DPPE-rhodamine (0.1 mol%) with a mixture of PfBro1:PfVps32 (1:2) together with PEG-FITC. The video is accelerated 4.5×.
(AVI)

S1 Supporting Materials and Methods. Supporting Materials and Methods.
(PDF)

Acknowledgments

We thank Dr. Elisabet Tintó-Font and Dr. Alfred Cortés for donating the plasmids that were used for our CRISPR/Cas9 constructs. Authors acknowledge Dr. Igor Florez-Sarasa for critical reading of this manuscript.

Author Contributions

Conceptualization: Yunuen Avalos-Padilla, René Verhoef, Lorenzo Albertazzi, Rumiana Dimova.

Data curation: Yunuen Avalos-Padilla, Silvia Pujals, René Verhoef.

Formal analysis: Yunuen Avalos-Padilla, Vasil N. Georgiev, Silvia Pujals, Rumiana Dimova.

Funding acquisition: Lorenzo Albertazzi, Rumiana Dimova, Xavier Fernández-Busquets.

Investigation: Yunuen Avalos-Padilla.

Methodology: Yunuen Avalos-Padilla, Vasil N. Georgiev, Elena Lantero, Silvia Pujals, René Verhoef, Livia N. Borgheti-Cardoso.

Project administration: Yunuen Avalos-Padilla, Xavier Fernández-Busquets.

Resources: Silvia Pujals, Lorenzo Albertazzi, Rumiana Dimova, Xavier Fernández-Busquets.

Software: Vasil N. Georgiev.

Supervision: Silvia Pujals, Rumiana Dimova, Xavier Fernández-Busquets.

Validation: Yunuen Avalos-Padilla, Vasil N. Georgiev, René Verhoef, Xavier Fernández-Busquets.

Visualization: Yunuen Avalos-Padilla, Silvia Pujals.

Writing – original draft: Yunuen Avalos-Padilla.

Writing – review & editing: Vasil N. Georgiev, Elena Lantero, Silvia Pujals, Livia N. Borgheti-Cardoso, Lorenzo Albertazzi, Rumiana Dimova, Xavier Fernández-Busquets.

References

1. WHO. World Malaria Report 2019. Geneva: World Health Organization; 2019. 232 pp]. Available from: <https://www.who.int/malaria/publications/world-malaria-report-2019/en/>.
2. Couper KN, Barnes T, Hafalla JCR, Combes V, Ryffel B, Secher T, et al. Parasite-Derived Plasma Microparticles Contribute Significantly to Malaria Infection-Induced Inflammation through Potent Macrophage Stimulation. *Plos Pathogens*. 2010;6(1). ARTN <https://doi.org/10.1371/journal.ppat.1000744> WOS:000274227100034. PMID: 20126448
3. Combes V, Taylor TE, Juhan-Vague I, Mege JL, Mwenechanya J, Tembo M, et al. Circulating endothelial microparticles in Malawian children with severe falciparum malaria complicated with coma. *Jama-*

- Journal of the American Medical Association. 2004; 291(21):2542–4. <https://doi.org/10.1001/jama.291.21.2542-b> WOS:000221738800014. PMID: 15173142
4. Mfonkeu JBP, Gouado I, Kuate HF, Zambou O, Zollo PHA, Grau GER, et al. Elevated Cell-Specific Microparticles Are a Biological Marker for Cerebral Dysfunctions in Human Severe Malaria. *Plos One*. 2010; 5(10). ARTN <https://doi.org/e1341510.1371/journal.pone.0013415> WOS:000282941000026.
 5. Campos FMF, Franklin BS, Teixeira-Carvalho A, Filho ALS, de Paula SCO, Fontes CJ, et al. Augmented plasma microparticles during acute *Plasmodium vivax* infection. *Malaria Journal*. 2010;9. ArtN 32710.1186/1475-2875-9-327. WOS:000287600800002. <https://doi.org/10.1186/1475-2875-9-9> PMID: 20064223
 6. Lauer SA, Rathod PK, Ghori N, Haldar K. A membrane network for nutrient import in red cells infected with the malaria parasite. *Science*. 1997; 276(5315):1122–5. <https://doi.org/10.1126/science.276.5315.1122> WOS:A1997WZ22500047. PMID: 9148808
 7. Akers JC, Gonda D, Kim R, Carter BS, Chen CC. Biogenesis of extracellular vesicles (EV): exosomes, microvesicles, retrovirus-like vesicles, and apoptotic bodies. *Journal of Neuro-Oncology*. 2013; 113(1):1–11. <https://doi.org/10.1007/s11060-013-1084-8> WOS:000318300700001. PMID: 23456661
 8. Schlacht A, Herman EK, Klute MJ, Field MC, Dacks JB. Missing Pieces of an Ancient Puzzle: Evolution of the Eukaryotic Membrane-Trafficking System. *Cold Spring Harbor Perspectives in Biology*. 2014; 6(10). ARTN a01604810.1101/cshperspect.a016048. WOS:000346448700007. <https://doi.org/10.1101/cshperspect.a016048> PMID: 25274701
 9. van Niel G D'Angelo G, Raposo G. Shedding light on the cell biology of extracellular vesicles. *Nat Rev Mol Cell Bio*. 2018; 19(4):213–28. <https://doi.org/10.1038/nrm.2017.125> WOS:000427924900008. PMID: 29339798
 10. Raposo G, Stoorvogel W. Extracellular vesicles: exosomes, microvesicles, and friends. *J Cell Biol*. 2013; 200(4):373–83. <https://doi.org/10.1083/jcb.201211138> PMID: 23420871; PubMed Central PMCID: PMC3575529.
 11. Winter V, Hauser MT. Exploring the ESCRTing machinery in eukaryotes. *Trends Plant Sci*. 2006; 11(3):115–23. Epub 2006/02/21. S1360-1385(06)00034-3 [pii]<https://doi.org/10.1016/j.tplants.2006.01.008> PMID: 16488176; PubMed Central PMCID: PMC2865992.
 12. Katzmann DJ, Odorizzi G, Emr SD. Receptor downregulation and multivesicular-body sorting. *Nat Rev Mol Cell Biol*. 2002; 3(12):893–905. Epub 2002/12/04. <https://doi.org/10.1038/nrm973> [pii]. PMID: 12461556.
 13. Raiborg C, Stenmark H. The ESCRT machinery in endosomal sorting of ubiquitylated membrane proteins. *Nature*. 2009; 458(7237):445–52. <https://doi.org/10.1038/nature07961> WOS:000264532400033. PMID: 19325624
 14. Katzmann DJ, Stefan CJ, Babst M, Emr SD. Vps27 recruits ESCRT machinery to endosomes during MVB sorting. *Journal of Cell Biology*. 2003; 162(3):413–23. <https://doi.org/10.1083/jcb.200302136> WOS:000184667900007. PMID: 12900393
 15. Gill DJ, Teo H, Sun J, Perisic O, Veprintsev DB, Emr SD, et al. Structural insight into the ESCRT-I/II link and its role in MVB trafficking. *Embo Journal*. 2007; 26(2):600–12. <https://doi.org/10.1038/sj.emboj.7601501> WOS:000243730700030. PMID: 17215868
 16. Im YJ, Wollert T, Boura E, Hurley JH. Structure and Function of the ESCRT-II-III Interface in Multivesicular Body Biogenesis. *Developmental Cell*. 2009; 17(2):234–43. <https://doi.org/10.1016/j.devcel.2009.07.008> WOS:000269138600013. PMID: 19686684
 17. Boura E, Rozycki B, Chung HS, Herrick DZ, Canagarajah B, Cafiso DS, et al. Solution Structure of the ESCRT-I and -II Supercomplex: Implications for Membrane Budding and Scission. *Structure*. 2012; 20(5):874–86. <https://doi.org/10.1016/j.str.2012.03.008> WOS:000304214400013. PMID: 22579254
 18. Babst M, Katzmann DJ, Snyder WB, Wendland B, Emr SD. Endosome-associated complex, ESCRT-II, recruits transport machinery for protein sorting at the multivesicular body. *Developmental Cell*. 2002; 3(2):283–9. [https://doi.org/10.1016/s1534-5807\(02\)00219-8](https://doi.org/10.1016/s1534-5807(02)00219-8) WOS:000177325700017. PMID: 12194858
 19. Teis D, Saksena S, Judson BL, Emr SD. ESCRT-II coordinates the assembly of ESCRT-III filaments for cargo sorting and multivesicular body vesicle formation. *Embo Journal*. 2010; 29(5):871–83. <https://doi.org/10.1038/emboj.2009.408> WOS:000275169800002. PMID: 20134403
 20. Obita T, Saksena S, Ghazi-Tabatabai S, Gill DJ, Perisic O, Emr SD, et al. Structural basis for selective recognition of ESCRT-III by the AAA ATPase Vps4. *Nature*. 2007; 449(7163):735–U11. <https://doi.org/10.1038/nature06171> WOS:000250045000047. PMID: 17928861
 21. Hurley JH. ESCRTs are everywhere. *Embo J*. 2015; 34(19):2398–407. <https://doi.org/10.15252/emboj.201592484> WOS:000362457800006. PMID: 26311197

22. Henne WM, Stenmark H, Emr SD. Molecular mechanisms of the membrane sculpting ESCRT pathway. *Cold Spring Harb Perspect Biol*. 2013; 5(9). Epub 2013/09/05. <https://doi.org/10.1101/cshperspect.a016766> [pii]5/9/a016766 [pii]. 24003212. PMID: 24003212
23. Leung KF, Dacks JB, Field MC. Evolution of the multivesicular body ESCRT machinery; retention across the eukaryotic lineage. *Traffic*. 2008; 9(10):1698–716. <https://doi.org/10.1111/j.1600-0854.2008.00797.x> WOS:000259238000013. PMID: 18637903
24. Dores MR, Paing MM, Lin H, Montagne WA, Marchese A, Trejo J. AP-3 regulates PAR1 ubiquitin-independent MVB/lysosomal sorting via an ALIX-mediated pathway. *Mol Biol Cell*. 2012; 23(18):3612–23. Epub 2012/07/27. <https://doi.org/10.1091/mbc.E12-03-0251> [pii]. PMID: 22833563; PubMed Central PMCID: PMC3442409.
25. Jimenez-Ruiz E, Morlon-Guyot J, Daher W, Meissner M. Vacuolar protein sorting mechanisms in apicomplexan parasites. *Molecular and Biochemical Parasitology*. 2016; 209(1–2):18–25. <https://doi.org/10.1016/j.molbiopara.2016.01.007> WOS:000390632200004. PMID: 26844642
26. Yang M, Coppens I, Wormsley S, Baeovova P, Hoppe HC, Joiner KA. The *Plasmodium falciparum* Vps4 homolog mediates multivesicular body formation. *Journal of Cell Science*. 2004; 117(17):3831–8. <https://doi.org/10.1242/jcs.01237> WOS:000223733100013. PMID: 15252121
27. Winter V, Hauser MT. Exploring the ESCRTing machinery in eukaryotes. *Trends in Plant Science*. 2006; 11(3):115–23. <https://doi.org/10.1016/j.tplants.2006.01.008> WOS:000236648200004. PMID: 16488176
28. Kim JW, Sitaraman S, Hierro A, Beach BM, Odorizzi G, Hurley JH. Structural basis for endosomal targeting by the Bro1 domain. *Developmental Cell*. 2005; 8(6):937–47. <https://doi.org/10.1016/j.devcel.2005.04.001> WOS:000230006200017. PMID: 15935782
29. Pick C, Ebersberger I, Spielmann T, Bruchhaus I, Burmester T. Phylogenomic analyses of malaria parasites and evolution of their exported proteins. *BMC Evol Biol*. 2011; 11:167. Epub 2011/06/17. <https://doi.org/10.1186/1471-2148-11-167> PMID: 21676252; PubMed Central PMCID: PMC3146879.
30. Mu R, Dussupt V, Jiang J, Sette P, Rudd V, Chuenchor W, et al. Two distinct binding modes define the interaction of Brox with the C-terminal tails of CHMP5 and CHMP4B. *Structure*. 2012; 20(5):887–98. Epub 2012/04/10. <https://doi.org/10.1016/j.str.2012.03.001> PMID: 22484091; PubMed Central PMCID: PMC3350598.
31. Pisitkun T, Shen RF, Knepper MA. Identification and proteomic profiling of exosomes in human urine. *Proc Natl Acad Sci U S A*. 2004; 101(36):13368–73. Epub 2004/08/25. <https://doi.org/10.1073/pnas.0403453101> PMID: 15326289; PubMed Central PMCID: PMC516573.
32. Babst M, Katzmann DJ, Estepa-Sabal EJ, Meerloo T, Emr SD. Escrt-III: an endosome-associated heterooligomeric protein complex required for mvb sorting. *Dev Cell*. 2002; 3(2):271–82. Epub 2002/08/27. [https://doi.org/10.1016/s1534-5807\(02\)00220-4](https://doi.org/10.1016/s1534-5807(02)00220-4) PMID: 12194857.
33. Avalos-Padilla Y, Knorr RL, Javier-Reyna R, Garcia-Rivera G, Lipowsky R, Dimova R, et al. The Conserved ESCRT-III Machinery Participates in the Phagocytosis of *Entamoeba histolytica*. *Frontiers in Cellular and Infection Microbiology*. 2018; 8. ARTN 5310.3389/fcimb.2018.00053. WOS:000426386400001. <https://doi.org/10.3389/fcimb.2018.00053> PMID: 29546036
34. Wollert T, Hurley JH. Molecular mechanism of multivesicular body biogenesis by ESCRT complexes. *Nature*. 2010; 464(7290):864–U73. <https://doi.org/10.1038/nature08849> WOS:000276397300031. PMID: 20305637
35. Virtanen JA, Cheng KH, Somerharju P. Phospholipid composition of the mammalian red cell membrane can be rationalized by a superlattice model. *P Natl Acad Sci USA*. 1998; 95(9):4964–9. <https://doi.org/10.1073/pnas.95.9.4964> WOS:000073415700034. PMID: 9560211
36. Bajorek M, Schubert HL, McCullough J, Langelier C, Eckert DM, Stubblefield WMB, et al. Structural basis for ESCRT-III protein autoinhibition. *Nature Structural & Molecular Biology*. 2009; 16(7):754–U95. <https://doi.org/10.1038/nsmb.1621> WOS:000267764500014. PMID: 19525971
37. Tang SG, Buchkovich NJ, Henne WM, Banjade S, Kim YJ, Emr SD. ESCRT-III activation by parallel action of ESCRT-I/II and ESCRT-0/Bro1 during MVB biogenesis. *Elife*. 2016; 5. ARTN e1550710.7554/eLife.15507. WOS:000376391800001. <https://doi.org/10.7554/eLife.15507> PMID: 27074665
38. Colombo M, Raposo G, Thery C. Biogenesis, Secretion, and Intercellular Interactions of Exosomes and Other Extracellular Vesicles. *Annual Review of Cell and Developmental Biology*, Vol 30. 2014; 30:255–89. <https://doi.org/10.1146/annurev-cellbio-101512-122326> WOS:000348434900012. PMID: 25288114
39. Matz JM, Beck JR, Blackman MJ. The parasitophorous vacuole of the blood-stage malaria parasite. *Nat Rev Microbiol*. 2020; 18(7):379–91. Epub 2020/01/26. <https://doi.org/10.1038/s41579-019-0321-3> PMID: 31980807.

40. Hiller NL, Bhattacharjee S, van Ooij C, Liolios K, Harrison T, Lopez-Estrano C, et al. A host-targeting signal in virulence proteins reveals a secretome in malarial infection. *Science*. 2004; 306(5703):1934–7. Epub 2004/12/14. <https://doi.org/10.1126/science.1102737> PMID: 15591203.
41. Chang HH, Falick AM, Carlton PM, Sedat JW, DeRisi JL, Marletta MA. N-terminal processing of proteins exported by malaria parasites. *Mol Biochem Parasitol*. 2008; 160(2):107–15. Epub 2008/06/07. <https://doi.org/10.1016/j.molbiopara.2008.04.011> PMID: 18534695; PubMed Central PMCID: PMC2922945.
42. Sampaio NG, Emery SJ, Garnham AL, Tan QY, Sisquella X, Pimentel MA, et al. Extracellular vesicles from early stage *Plasmodium falciparum*-infected red blood cells contain PfEMP1 and induce transcriptional changes in human monocytes. *Cell Microbiol*. 2018; 20(5):e12822. Epub 2018/01/20. <https://doi.org/10.1111/cmi.12822> PMID: 29349926.
43. Regev-Rudzki N, Wilson DW, Carvalho TG, Sisquella X, Coleman BM, Rug M, et al. Cell-Cell Communication between Malaria-Infected Red Blood Cells via Exosome-like Vesicles. *Cell*. 2013; 153(5):1120–33. <https://doi.org/10.1016/j.cell.2013.04.029> WOS:000319456800018. PMID: 23683579
44. Babatunde KA, Subramanian BY, Ahouidi AD, Murillo PM, Walch M, Mantel PY. Role of Extracellular Vesicles in Cellular Cross Talk in Malaria. *Front Immunol*. 2020; 11. ARTN 22 <https://doi.org/10.3389/fimmu.2020.00022> WOS:000512689100001. PMID: 32082312
45. Colombo M, Moita C, van Niel G, Kowal J, Vigneron J, Benaroch P, et al. Analysis of ESCRT functions in exosome biogenesis, composition and secretion highlights the heterogeneity of extracellular vesicles. *Journal of Cell Science*. 2013; 126(24):5553–65. <https://doi.org/10.1242/jcs.128868> WOS:000328686600003. PMID: 24105262
46. Booth AM, Fang Y, Fallon JK, Yang JM, Hildreth JEK, Gould SJ. Exosomes and HIV Gag bud from endosome-like domains of the T cell plasma membrane. *Journal of Cell Biology*. 2006; 172(6):923–35. <https://doi.org/10.1083/jcb.200508014> WOS:000235971900017. PMID: 16533950
47. Odorizzi G, Katzmann DJ, Babst M, Audhya A, Emr SD. Bro1 is an endosome-associated protein that functions in the MVB pathway in *Saccharomyces cerevisiae*. *Journal of Cell Science*. 2003; 116(10):1893–903. <https://doi.org/10.1242/jcs.00395> WOS:000183098900005. PMID: 12668726
48. Goldberg DE. Plasmodium protein export at higher PEXEL resolution. *Cell Host Microbe*. 2012; 12(5):609–10. Epub 2012/11/20. <https://doi.org/10.1016/j.chom.2012.11.001> PMID: 23159050.
49. Booth A, Marklew CJ, Ciani B, Beales PA. In Vitro Membrane Remodeling by ESCRT is Regulated by Negative Feedback from Membrane Tension. *Iscience*. 2019; 15:173–+. <https://doi.org/10.1016/j.isci.2019.04.021> WOS:000470104600016. PMID: 31060000
50. Mierzwa BE, Chiaruttini N, Redondo-Morata L, von Filseck JM, König J, Larios J, et al. Dynamic subunit turnover in ESCRT-III assemblies is regulated by Vps4 to mediate membrane remodelling during cytokinesis. *Nature Cell Biology*. 2017; 19(7):787–+. <https://doi.org/10.1038/ncb3559> WOS:000404408800011. PMID: 28604678
51. Adell MAY, Migliano SM, Upadhyayula S, Bykov YS, Sprenger S, Pakdel M, et al. Recruitment dynamics of ESCRT-III and Vps4 to endosomes and implications for reverse membrane budding. *Elife*. 2017; 6. ARTN e31652. <https://doi.org/10.7554/eLife.31652> WOS:000414139400001. PMID: 29019322
52. Morita E, Sandrin V, Chung HY, Morham SG, Gygi SP, Rodesch CK, et al. Human ESCRT and ALIX proteins interact with proteins of the midbody and function in cytokinesis. *Embo Journal*. 2007; 26(19):4215–27. <https://doi.org/10.1038/sj.emboj.7601850> WOS:000250466800004. PMID: 17853893
53. Piper RC, Cooper AA, Yang H, Stevens TH. VPS27 controls vacuolar and endocytic traffic through a prevacuolar compartment in *Saccharomyces cerevisiae*. *J Cell Biol*. 1995; 131(3):603–17. Epub 1995/11/01. <https://doi.org/10.1083/jcb.131.3.603> PMID: 7593183; PubMed Central PMCID: PMC2120612.
54. Raymond CK, Howald-Stevenson I, Vater CA, Stevens TH. Morphological classification of the yeast vacuolar protein sorting mutants: evidence for a prevacuolar compartment in class E vps mutants. *Mol Biol Cell*. 1992; 3(12):1389–402. Epub 1992/12/01. <https://doi.org/10.1091/mbc.3.12.1389> PMID: 1493335; PubMed Central PMCID: PMC275707.
55. Matthews KM, Pitman EL, de Koning-Ward TF. Illuminating how malaria parasites export proteins into host erythrocytes. *Cell Microbiol*. 2019; 21(4):e13009. Epub 2019/01/19. <https://doi.org/10.1111/cmi.13009> PMID: 30656810.
56. Mantel PY, Hoang AN, Goldowitz I, Potashnikova D, Hamza B, Vorobjev I, et al. Malaria-Infected Erythrocyte-Derived Microvesicles Mediate Cellular Communication within the Parasite Population and with the Host Immune System. *Cell Host & Microbe*. 2013; 13(5):521–34. <https://doi.org/10.1016/j.chom.2013.04.009> WOS:000330850800006. PMID: 23684304
57. Lambros C, Vanderberg JP. Synchronization of *Plasmodium falciparum* Erythrocytic Stages in Culture. *Journal of Parasitology*. 1979; 65(3):418–20. <https://doi.org/10.2307/3280287> WOS: A1979HK51700015. PMID: 383936

58. Mehnert AK, Simon CS, Guizetti J. Immunofluorescence staining protocol for STED nanoscopy of Plasmodium-infected red blood cells. *Molecular and Biochemical Parasitology*. 2019; 229:47–52. <https://doi.org/10.1016/j.molbiopara.2019.02.007> WOS:000465052800006. PMID: 30831155
59. Nahidiazar L, Agronskaia AV, Broertjes J, van den Broek B, Jalink K. Optimizing Imaging Conditions for Demanding Multi-Color Super Resolution Localization Microscopy. *Plos One*. 2016; 11(7). ARTN e0158884. <https://doi.org/10.1371/journal.pone.0158884> PMID: 27391487
60. Weinberger A, Tsai FC, Koenderink GH, Schmidt TF, Itri R, Meier W, et al. Gel-assisted formation of giant unilamellar vesicles. *Biophys J*. 2013; 105(1):154–64. Epub 2013/07/05. <https://doi.org/10.1016/j.bpj.2013.05.024> PMID: 23823234; PubMed Central PMCID: PMC3699747.
61. Maan R, Loiseau E, Bausch AR. Adhesion of Active Cytoskeletal Vesicles. *Biophys J*. 2018; 115(12):2395–402. Epub 2018/11/21. <https://doi.org/10.1016/j.bpj.2018.10.013> PubMed Central PMCID: PMC6301914. PMID: 30455042
62. Ghorbal M, Gorman M, Macpherson CR, Martins RM, Scherf A, Lopez-Rubio JJ. Genome editing in the human malaria parasite *Plasmodium falciparum* using the CRISPR-Cas9 system. *Nat Biotechnol*. 2014; 32(8):819–21. Epub 2014/06/02. <https://doi.org/10.1038/nbt.2925> PMID: 24880488
63. Llorca-Batlle O, Michel-Todo L, Witmer K, Toda H, Fernandez-Becerra C, Baum J, et al. Conditional expression of PfAP2-G for controlled massive sexual conversion in *Plasmodium falciparum*. *Sci Adv*. 2020; 6(24):eaaz5057. Epub 2020/06/25. <https://doi.org/10.1126/sciadv.aaz5057> PMID: 32577509; PubMed Central PMCID: PMC7286680.
64. Lim MY, LaMonte G, Lee MCS, Reimer C, Tan BH, Corey V, et al. UDP-galactose and acetyl-CoA transporters as *Plasmodium* multidrug resistance genes. *Nat Microbiol*. 2016; 1:16166. Epub 2016/09/20. <https://doi.org/10.1038/nmicrobiol.2016.166> PMID: 27642791; PubMed Central PMCID: PMC5575994.
65. Knuepfer E, Napiorkowska M, van Ooij C, Holder AA. Generating conditional gene knockouts in *Plasmodium*—a toolkit to produce stable DiCre recombinase-expressing parasite lines using CRISPR/Cas9. *Sci Rep*. 2017; 7(1):3881. Epub 2017/06/22. <https://doi.org/10.1038/s41598-017-03984-3> PMID: 28634346; PubMed Central PMCID: PMC5478596.
66. Rovira-Graells N, Gupta AP, Planet E, Crowley VM, Mok S, Ribas de Pouplana L, et al. Transcriptional variation in the malaria parasite *Plasmodium falciparum*. *Genome Res*. 2012; 22(5):925–38. Epub 2012/03/15. <https://doi.org/10.1101/gr.129692.111> PMID: 22415456; PubMed Central PMCID: PMC3337437.
67. Borgheti-Cardoso LN, Kooijmans SAA, Chamorro LG, Biosca A, Lantero E, Ramirez M, et al. Extracellular vesicles derived from *Plasmodium*-infected and non-infected red blood cells as targeted drug delivery vehicles. *Int J Pharm*. 2020; 587:119627. Epub 2020/07/13. <https://doi.org/10.1016/j.ijpharm.2020.119627> PMID: 32653596.
68. Hubert A, Subra C, Jenabian MA, Tremblay Labrecque PF, Tremblay C, Laffont B, et al. Elevated Abundance, Size, and MicroRNA Content of Plasma Extracellular Vesicles in Viremic HIV-1+ Patients: Correlations With Known Markers of Disease Progression. *J Acquir Immune Defic Syndr*. 2015; 70(3):219–27. Epub 2015/07/17. <https://doi.org/10.1097/QAI.0000000000000756> PMID: 26181817; PubMed Central PMCID: PMC4627170.
69. Gray R, Albrecht D. Super-resolution Microscopy of Vaccinia Virus Particles. *Methods Mol Biol*. 2019; 2023:255–68. Epub 2019/06/27. https://doi.org/10.1007/978-1-4939-9593-6_16 PMID: 31240683.